Nanoscale Advances

ROYAL SOCIETY OF CHEMISTRY

REVIEW

View Article Online
View Journal | View Issue

Cite this: *Nanoscale Adv.*, 2024, **6**, 4504

Controlled synthesis, properties, and applications of ultralong carbon nanotubes

Kangkang Wang, Fei Wang, Qinyuan Jiang, Ping Zhu, Khaixien Leu and Rufan Zhang *

Carbon nanotubes (CNTs) are typical one-dimensional nanomaterials which have been widely studied for more than three decades since 1991 because of their excellent mechanical, electrical, thermal, and optical properties. Among various types of CNTs, the ultralong CNTs which have lengths over centimeters and defect-free structures exhibit superior advantages for fabricating superstrong CNT fibers, CNT-based chips, transparent conductive films, and high-performance cables. The length, orientation, alignment, defects, cleanliness, and other microscopic characteristics of CNTs have significant impacts on their fundamental physical properties. Therefore, the controlled synthesis and mass production of high-quality ultralong CNTs is the key to fully exploiting their extraordinary properties. Despite significant progress made in the study of ultralong CNTs during the past three decades, the precise structural control and mass production of ultralong CNTs remain a great challenge. In this review, we systematically summarize the growth mechanism and controlled synthesis strategies of ultralong CNTs. We also introduce the progress in the applications of ultralong CNTs. Additionally, we summarize the scientific and technological challenges facing the mass production of ultralong CNTs and provide an outlook and in-depth discussion on the future development direction.

Received 27th May 2024
Accepted 24th June 2024

DOI: 10.1039/d4na00437j

rsc.li/nanoscale-advances

1. Introduction

Carbon nanotubes (CNTs) are one-dimensional Dirac materials that have exceptional electrical, mechanical, optical, and thermal properties.[1–3] CNTs have wide applications in many cutting-edge fields such as carbon-based integrated circuits, super-strong fibers, sensing, mechanical energy storage, and flexible wearable devices, *etc.*[4–8] For instance, CNTs have a very high Young's modulus of up to 1 TPa and a high tensile strength of up to 100 GPa, which far exceeds that of steel.[9] Furthermore, CNTs have excellent electrical conductivity which can withstand a current density of up to 10^9 A cm^{-2}, much higher than that of copper wires.[5,10] Additionally, CNTs have unique electromagnetic properties and can be used to make high-frequency electronic devices and electromagnetic shielding materials.[11,12] CNTs have shown promising application prospects in fields such as aerospace, information technology, energy storage, environment protection, military, and biomedicine.[13–16] Among the various factors affecting the properties and performance of CNTs, the length, defect concentration, crystallinity, chirality, and alignment of CNTs are the most significant ones.[5–7] Especially, the length of individual CNTs is a critical factor which determines the properties of macroscopic CNT fibers and films, *e.g.*, their electrical conductivity, thermal conductivity, tensile strength, and tensile strain, *etc.*[8] Therefore, it is highly significant to make individual CNTs as long as possible. According to the differences in the alignments, lengths, and morphologies of CNTs, they can be divided into three different categories, which are agglomerated CNTs, vertically aligned CNT arrays (VACNTs), and horizontally aligned CNT arrays (HACNTs).[9] Generally, the agglomerated CNTs and VACNTs have short lengths shorter than a millimeter and many structural defects.[10–17] In comparison, the HACNTs usually grow on flat substrates and have very few structural defects, which render them with excellent electrical, mechanical, and thermal properties.[9] Moreover, the HACNTs can also be further categorized into two sub-types based on their different growth mechanisms. The first kind of HACNTs is usually grown on substrates such as quartz[18,19] and single crystal MgO[20] with a base-growth mechanism. The base-growth HACNTs are also typically less than one millimeter in length and grow slowly.[21,22] In contrast, the second kind of HACNTs are grown on silicon substrates with a flying kite-like tip-growth mechanism.[23–29] The tip-growth HACNTs have very fast growth rates and their lengths can be as long as several centimeters or even several decimeters,[9,30] which are much longer than other types of CNTs. Therefore, the tip-growth HACNTs are usually called "ultralong CNTs".[8,30,31] Because of the macroscale lengths, good alignment, perfect structures, and excellent properties, ultralong CNTs are ideal candidates for fabricating CNT fibers, transparent conductive films, conductive wires, and carbon-based integrated circuits.[8]

Department of Chemical Engineering, Tsinghua University, Beijing 100084, China. E-mail: zhangrufan@tsinghua.edu.cn

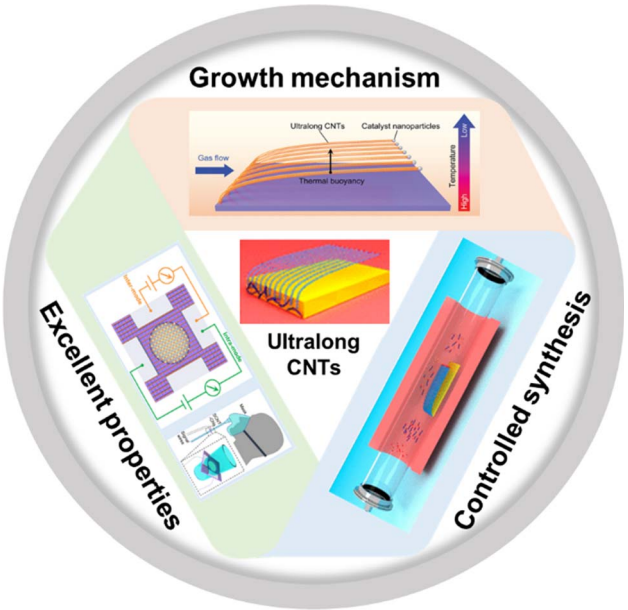

Fig. 1 Growth mechanism, controlled synthesis, and excellent properties of ultralong CNTs.[30,31,33] Reproduced from ref. 30 with permission from Wiley-VCH, copyright 2023. Reproduced from ref. 31 with permission from American Chemical Society, copyright 2023. Reproduced from ref. 33 with permission from American Chemical Society, copyright 2024.

However, the biggest challenge facing ultralong CNTs is how to realize their mass production. The yields of ultralong CNTs are usually much lower than that of other types of CNTs, which severely hinders their application in various fields. Besides, it is also essential to overcome the challenges like precise structural and morphological control the high cost, and the functionalization of CNT fibers.[17–20,32] It is worth noting that many cutting-edge fields propose very stringent requirements on the structure of CNTs.[21] For example, transparent conductive films, electrothermal films, and CNT fibers usually require CNTs with longer monomer lengths to reduce contact thermal and electrical resistance, and enhance stress transfer between tubes.[22–24] In carbon-based integrated circuit applications, CNTs with good orientation are necessary to construct tunneling transistor structures.[25,26] Therefore, achieving controlled synthesis of CNTs with macroscopic size, high crystallinity, and low defect density is crucial for their wide applications.[27–29]

In the past two decades, people have successfully prepared ultralong CNTs with macroscopic lengths, perfect structures, controlled morphologies, and excellent properties. Many efforts have been made in the study of the growth mechanism, synthesis methods, property study, and application exploitation of ultralong CNTs (Fig. 1).[30,31,33] In this paper, we review recent research progress on the controlled preparation of ultralong CNTs and their properties. We also analyze the challenges and future development directions. This review is expected to provide more inspiration and reference for the mass production and future development of ultralong CNTs.

2. Growth mechanism of ultralong CNTs

There are three main methods for synthesizing CNTs: arc discharge, laser ablation, and chemical vapor deposition (CVD).[34–37] Among them, the CVD methods have shown many advantages in controlling the structure and morphology, specific orientation growth, and mass production of CNTs.[38] After decades of development, CVD has become a mature technology for the preparation of various thin films and nanomaterials.[39,40] This section mainly discusses the CVD growth mechanism of ultralong CNTs.

2.1. Mechanism for nucleation and growth of general CNTs

The mechanism of nucleation and growth of CNTs is a complex physicochemical process involving the arrangement and assembly of carbon atoms on the nanoscale.[41–43] Nucleation is the first stage of CNT growth, where carbon atoms form the initial tubular structure on the substrate surface.[44] In this process, carbon atoms must first be adsorbed on the substrate surface and then aggregated into a nucleation under suitable conditions through surface diffusion.[45] This nucleus is typically a ring structure that consists of a few carbon atoms that are hybridized by sp^2 to form a six-membered ring, which is connected by σ-bonds.[46] As the nucleus grows, carbon atoms continue to adsorb and join the ring structure, turning it into a tube. After nucleation, CNTs enter the growth phase, where the key is how the carbon atoms are deposited along the tube wall in a specific orientation.[47,48]

After adsorption on the surface, carbon atoms can be added to the growing CNTs in three different ways. (1) Additive method: hydrocarbons like methane or hydrogen are usually used as carbon sources in the CVD process. Carbon atoms first react with hydrogen atoms to form small molecules such as methane, which then decompose at high temperatures. This releases carbon atoms that stick to the surface of the nanotubes and grow along the tube walls. (2) Catalytic growth: catalysts like iron, nickel, or cobalt are pre-coated on the substrates. Carbon atoms react with these catalyst particles at high temperatures to produce CNTs. The catalyst plays an important role by providing a suitable surface and active sites for carbon atoms to nucleate and grow. (3) Free radical growth: this method involves the decomposition of hydrocarbon molecules to produce free radicals under plasma or laser irradiation. These free radicals then migrate and deposit carbon atoms on the surface, promoting the growth of CNTs.[49–52] It is important to note that temperature, pressure, gas flow, catalyst selection, and other factors can significantly impact the growth of CNTs.[53] By controlling these conditions, it is possible to modulate the structure (*e.g.*, wall number, diameter, length) and properties (*e.g.*, mechanical, electrical, and chemical) of CNTs to a certain extent.[54]

2.2. Mechanism for base-growth and tip-growth mode of CNTs

Understanding the growth mechanisms and modes of CNTs is essential to control their structures.[55] As shown in Fig. 2a, the

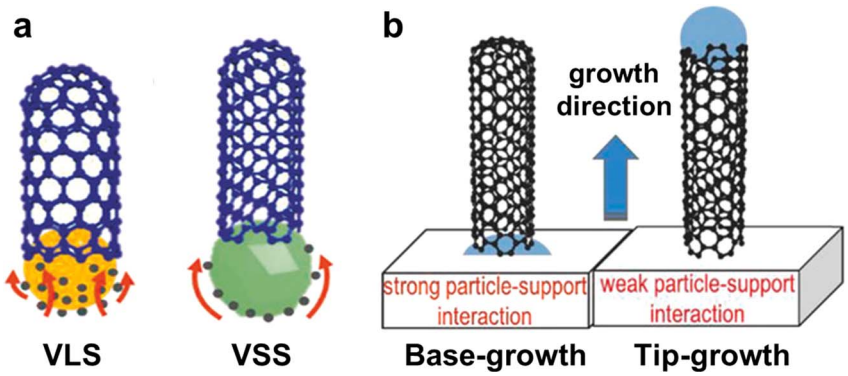

Fig. 2 (a) Schematic diagram of the VLS and VSS growth mechanisms of CNTs. (b) Diagram of base-growth and tip-growth modes of CNTs.[56] Reproduced from ref. 56 with permission from Wiley-VCH, copyright 2019.

CVD process can be divided into two mechanisms based on the phase states of the catalysts: vapor–liquid–solid (VLS) and vapor–solid–solid (VSS).[56] Researchers proposed two main growth modes to understand the growth behaviors of CNTs: tip-growth and base-growth modes (Fig. 2b).[56,57] These growth modes are proposed to describe the motion behavior of the catalysts and the forces between the catalysts and substrates during the growth of CNTs.

2.2.1. Base-growth mode of CNTs. The base-growth mode is a method for growing CNTs where the catalyst particles remain on the substrate surface, while the tips of the CNTs grow away from the catalyst.[58] In this mode, the growth of CNTs can be influenced by factors such as the airflow, heat, supply, and diffusion of carbon source, which can affect the activity of the catalysts and their bonding with the substrates.[59,60] This can lead to catalyst deactivation and uneven growth of CNTs. Typically, CNTs grown in this mode tend to be short in length and show irregular distribution when the substrate induction is weak.[61] Homma *et al.* used transmission electron microscopy (TEM) to observe the *in situ* growth of CNTs at 600 °C with acetylene as a carbon source.[62] The catalysts and the carrier were close together, while the CNTs were nucleated on the catalyst and their tips were gradually growing outwards away from the catalyst. Using isotopic labeling, Ago *et al.* found that CNTs prepared on quartz sheets oriented by the lattice also relied mainly on the base-growth mode.[63] Similarly, He *et al.* demonstrated that CNTs prepared on SiO_2/Si substrates also followed the base-growth mode by calcining the catalyst on which the CNTs had been grown in air to regrow CNTs.[59] In conclusion, the strong force between the substrate and the catalyst leads to the base-growth mode of CNTs.

The base-growth mode of CNTs is mainly influenced by low temperatures.[64] There are two reasons for this phenomenon. Firstly, the lower temperature makes the catalyst particles have larger sizes which is better for them to infiltrate the substrate surface, creating a stronger force. This makes it difficult for the catalysts to leave the substrate when CNTs are grown, which ultimately leads to the emergence of the base-growth mode.[65] Secondly, the temperature difference between the substrate and the gas flow caused by the low temperature is smaller, which weakens the effect of thermal buoyancy and thus makes it difficult for the catalyst to be lifted and enter the laminar zone of the gas flow.[66] In addition to the temperature, the types of catalysts and their melting points also affect the growth modes of CNTs.[67] Concretely, catalysts with low melting points are more likely to present a liquid state and show poorer wettability on the substrates, leading to a tip-growth mode of CNTs. However, catalysts with high melting points always maintain a near-solid state, have poorer mobility, a stronger force with the substrates, and show better wettability on the substrate surface, resulting in a base-growth mode.

2.2.2. Tip-growth mode of CNTs. The tip-growth mode means that a part of the CNTs is located on the surface of the substrate during the growth process.[68] The catalyst is located at the tip of the CNTs and floats in the airflow, catalyzing the growth of CNTs in the direction of the airflow. This mode allows the CNTs to grow freely and makes it easier to grow horizontal arrays of CNTs with perfect structures and macroscopic lengths. Many experimental results have verified that the horizontal arrays of CNTs prepared by the airflow-induced methods follow the tip-growth mode. Li *et al.* proposed a "kite mechanism" to explain the tip-growth mode of CNTs along the airflow-induced directional growth.[57] The difference in the heating rate between the substrate and the airflow during the growth process creates a temperature difference perpendicular to the substrate, which generates a thermal buoyancy force. This force causes a portion of CNTs to be lifted off from the substrate and float in the reactive gas stream, while the catalyst at the tip of the CNTs causes them to grow in the direction of the gas stream. Further, catalyst particles are found at the growing end of the CNTs, verifying that the airflow induces the horizontal array of oriented CNTs to follow the apical growth pattern.[69]

Tip-growth mode is a better way to generate horizontal arrays of CNTs that have a perfect structure and macroscopic length.[70] These arrays can be utilized to create super-strong macroscopic materials. In this mode, the CNTs float in a reactive gas flow that is laminar, making it easier for them to contact and react with carbon source molecules. This results in CNTs with a high growth rate.[71] Furthermore, the growth of CNTs in the airflow is not easily interfered with or controlled by the substrate, which

avoids excessive defects, thus obtaining CNTs with a more perfect structure. In contrast, CNTs are more prone to create defects and be shorter in length *via* base-growth mode due to the limitations of the substrate and the mass transfer resistance during the growth process.

In summary, there are two main growth modes for CNTs, which are base-growth mode and tip-growth mode. In the actual growth process, the two growth modes usually coexist, especially in the horizontal array growth of CNTs. Because it is challenging to maintain the catalyst's morphology and the microenvironment consistent. Tip-growth mode is more suitable for producing ultralong CNTs with faster growth rates and macroscale lengths.[17] This is because high growth rates require a substantial amount of carbon source molecules in the gas phase to decompose on the surface of the catalyst particles. Catalyst particles that float in the gas stream are more likely to satisfy this condition than immobile particles on the substrate. The immobile catalyst particles' catalytic activity is more likely to be disrupted by the substrate, and the mass transfer resistance on the surface is also more significant than that of catalyst particles floating in the gas stream.

2.3. Growth mechanism of ultralong CNTs

Horizontal arrays of CNTs can be prepared through either base-growth mode or tip-growth mode. In the base-growth mode, the CNTs grow on single-crystal quartz or sapphire substrates and follow a crawling growth pattern.[72,73] While this method can produce arrays with high areal density and high orientation, the growth process is hindered by van der Waals forces on the substrate.[74] Consequently, the CNTs have slow growth rates and have a limited length shorter than 0.1 mm.[75] This is insufficient for many applications that require CNTs with macroscale lengths. In contrast, the tip-growth mode uses a unique "kite-like growth" mechanism.[57] Specifically, the CNTs are subjected to the synergistic effects of drag force, thermal buoyancy, and van der Waals force. One end of a CNT is fixed to the substrate while the other end with a catalyst particle floats in the gas phase. This method can produce horizontal arrays of ultralong CNTs with lengths of up to centimeters or even decimeters. Significant progress has been made in the synthesis of ultralong CNTs over the past two decades (Fig. 3).[7,30,31,76–81] These ultralong CNTs are better suited for many applications due to their superior performance.

In the tip-growth process of ultralong CNTs, the catalysts collide with gas molecules in the gas phase. This collision enhances the reaction and mass transfer process, leading to a growth rate of up to 80–90 μm s^{-1}.[82] The growth process is almost unaffected by the substrate, which enables carbon atoms to be assembled rapidly and precisely at the interface between the catalysts and the CNTs. This results in a defect-free structure with a length of up to 65 cm.[79] Moreover, the airflow traction can provide good orientation for the ultralong CNTs, allowing them to form a well-oriented array along the flow line.

During the tip-growth mode of ultralong CNTs, thermal buoyancy force plays an essential role in making the CNTs be

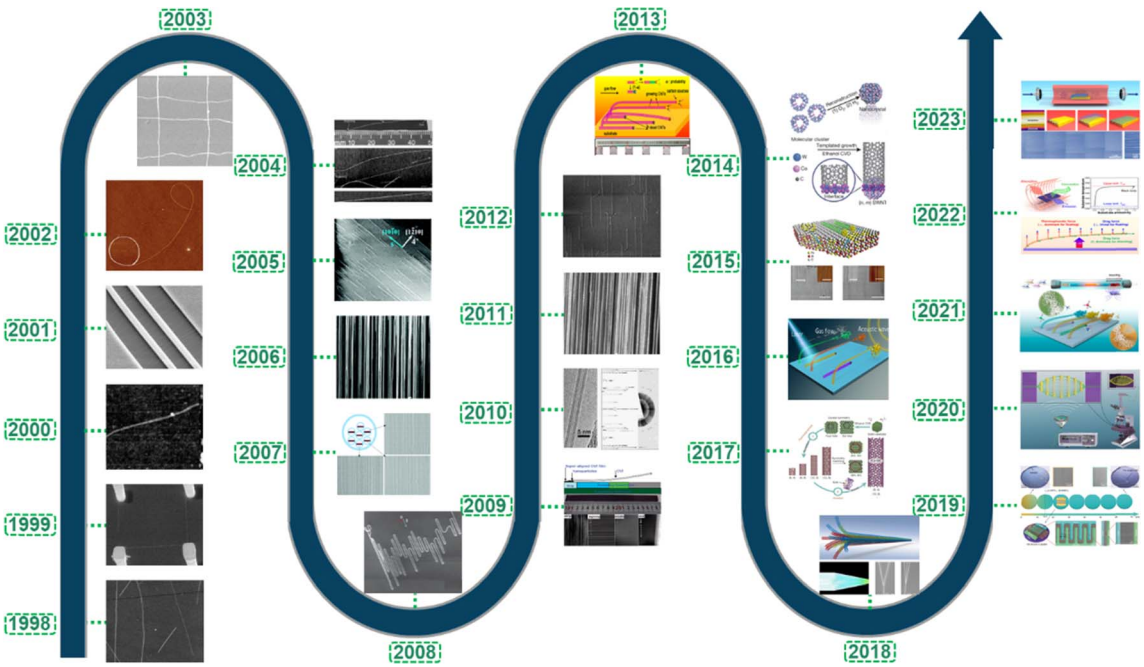

Fig. 3 Timeline of major milestones in the controlled synthesis of ultralong CNTs.[7,30,31,76–81] Reproduced from ref. 7 with permission from Royal Society of Chemistry, copyright 2017. Reproduced from ref. 30 with permission from Wiley-VCH, copyright 2022. Reproduced from ref. 31 with permission from American Chemical Society, copyright 2023. Reproduced from ref. 76 with permission from Springer Nature, copyright 2004. Reproduced from ref. 77 with permission from Springer Nature, copyright 2017. Reproduced from ref. 78 with permission from Springer Nature, copyright 2018. Reproduced from ref. 79 with permission from Springer Nature, copyright 2019. Reproduced from ref. 80 with permission from American Association for the Advancement of Science, copyright 2020. Reproduced from ref. 81 with permission from American Chemical Society, copyright 2021.

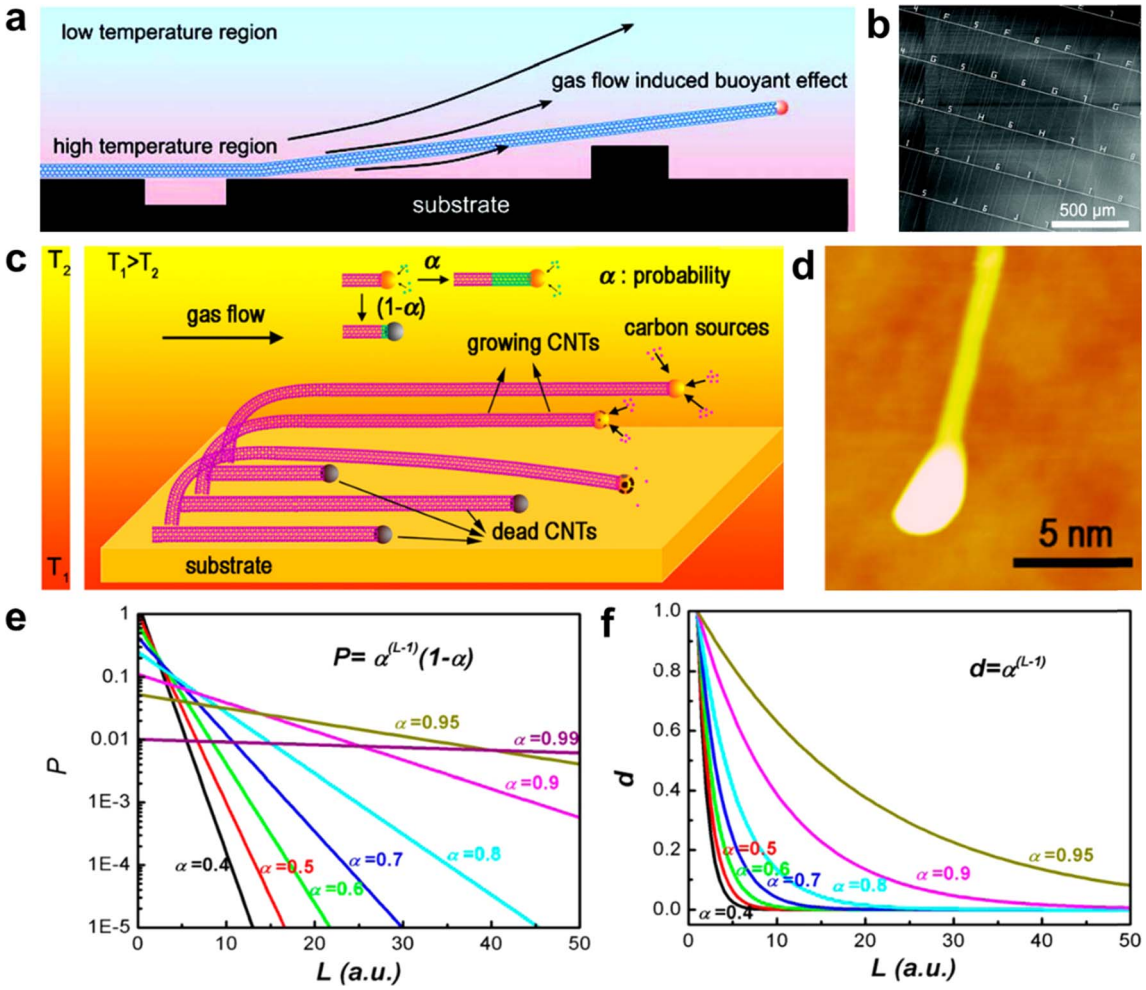

Fig. 4 (a) Schematic illustration of the tip-growth mechanism of ultralong CNTs. (b) SEM image of SWCNT arrays grown across microtrenches.[57] Reproduced from ref. 57 with permission from American Chemical Society, copyright 2007. (c) Illustration of tip-growth of ultralong CNTs based on Schulz–Flory distribution. (d) Atomic force microscopy image of a CNT with a catalyst nanoparticle on its tip. (e) Theoretical percentage and (f) theoretical number density of ultralong CNTs.[84] Reproduced from ref. 84 with permission from American Chemical Society, copyright 2013.

lifted off from the substrate surface. This force is generated by the temperature difference between the substrate and the surrounding airflow.[30] The catalyst particles located at the tip of the CNTs remain unaffected by the substrate wall effect and can directly contact the carbon source in the gas. This allows for the high-speed growth of defect-free CNTs. However, there are two unsolved issues in the growth system of ultralong CNTs, which are (1) the reason for the temperature difference between the substrate and the gas stream, and (2) the nature of thermal buoyancy.

Researchers have proposed several explanations for the temperature difference observed between the substrate and the airflow during the preparation of ultralong CNTs. Liu *et al.* believed that the temperature difference was caused by the difference in heating rates between the substrate and the airflow.[64] Zhang *et al.* further extended this theory to other synthesis methods.[83] Li *et al.* pointed out that the substrate was significantly heated by the heat conduction and the radiation from the reactor wall, resulting in a substantial temperature difference with the cold air flow from upstream (Fig. 4a and b).[57] Although these theories explained some experimental phenomena and provided guidance for experimental design, they did not offer a quantitative relationship between the temperature difference and the growth conditions (such as growth temperature, gas flow rate, and substrate material). The spiral growth theory of CNTs suggests that ultralong CNTs can be considered as a linear carbon polymer. Zhang *et al.* found that their growth follows the Schulz–Flory (SF) distribution.[84,85] The probability of the catalyst particles remaining active enough to support the growth of CNTs when the unit length was increased was defined as α (Fig. 4c). Both theoretical calculations and experimental results demonstrated that, regardless of α, the number density of CNTs decreases irreversibly as their length increases, which is an irreversible trend (Fig. 4d–f). To increase the number density and length of ultralong CNTs, the value of α should be increased as much as possible. This theory successfully explains the growth mechanism of ultralong CNT arrays.

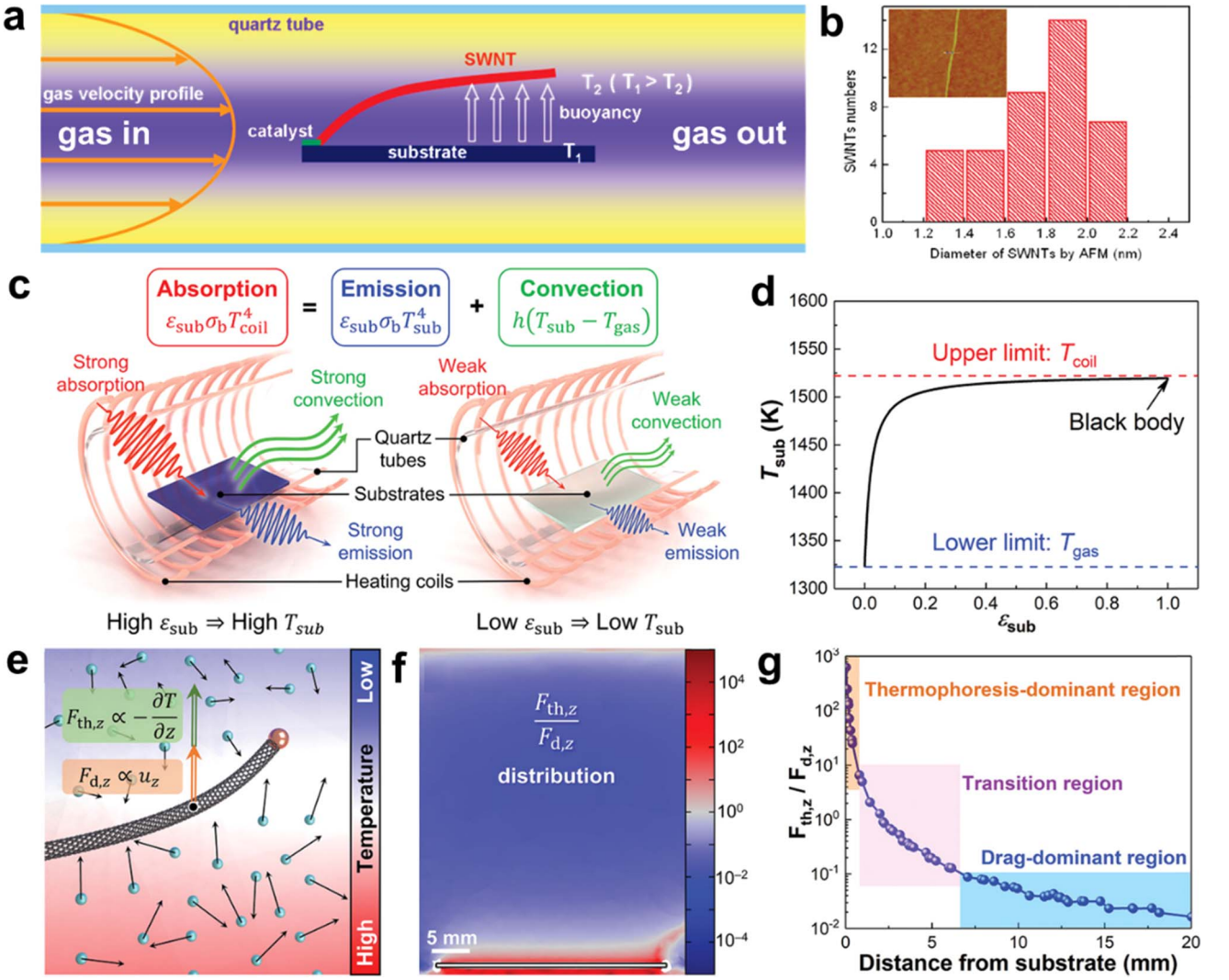

Fig. 5 (a) Schematic diagram of the formation mechanism of thermal buoyancy. (b) Diameter distribution of SWCNTs by AFM. The inset is a typical AFM image of an individual SWCNT.[83] Reproduced from ref. 83 with permission from American Chemical Society, copyright 2010. (c) Schematic illustration of the heat balance of the substrates with different emissivity. (d) Relationship between substrate temperature and substrate emissivity. (e) Thermophoretic force and drag force applied on a CNT in a non-uniform temperature field. (f) Distribution of the ratio of thermophoretic force to drag force in the vertical direction. (g) Distribution of the dominant regions of thermophoresis and drag.[30] Reproduced from ref. 30 with permission from Wiley-VCH, copyright 2023.

Previous studies have assumed that thermal buoyancy is due to natural convection (Fig. 5a and b).[83,86] When there is a temperature difference between the substrate and the airflow, the air close to the substrate gets heated, creating a density gradient that drives natural convection. This causes the warmer gas to move upwards, lifting the CNTs and causing them to float above the substrate. However, this theory can only explain the growth of ultralong CNTs on horizontally placed substrates as the traction force due to natural convection is directly related to the direction of the density gradient. However, experimental studies have shown that ultralong CNTs can also be grown on vertical substrates.[86] The direction of the thermal buoyancy force in this case does not coincide with the direction of the trailing force due to natural convection. This indicates that the theory is still incomplete and cannot fully explain the existing experimental phenomena.

Zhang *et al.* first proposed a solution to two problems related to the growth of ultralong CNTs on flat substrates. They introduced the concept of the inherent thermal effect of the substrates and developed a heat balance model that describes the heat transfer behavior between the substrate and the surrounding environment (Fig. 5c and d).[30] The model consists of absorption, emission, and convection. Based on this model, they found that the substrate temperature is higher than the airflow, and the substrate temperature is positively correlated with its emissivity. This explains the difference in the growth pattern of CNTs on single-crystal silicon and quartz substrates. Silicon has a high emissivity, which produces a strong intrinsic thermal effect of the substrate and thus a strong thermal buoyancy effect in its vertical direction, which is beneficial for the floating growth of CNTs.[84] In contrast, quartz has a very low emissivity and a weak thermal buoyancy effect in its vertical

direction, which is unfavorable for the floating growth of CNTs.[87] In addition, the researchers analyzed the natural convection and thermophoresis phenomena induced by temperature gradients using computational fluid dynamics simulations (Fig. 5e–g). They quantified the relative magnitudes of the trailing and thermophoretic forces due to natural convection. By combining theoretical calculations with experiments, they proved that the thermophoretic force is the main driving force to make the CNTs float from the substrate. The direction of the thermophilic force is opposite to that of the temperature gradient and independent of the direction of the velocity of the airflow. It provides a lifting force perpendicular to the surface of the substrate for a long period for the ultralong CNTs, which can explain their growth behavior on the vertical substrate. Finally, they applied the theory of the intrinsic thermal effect of the substrate to the reactor design and artificially set the temperature gradient in the vertical or horizontal direction. This allowed them to realize the precise regulation of the density and orientation of ultralong CNT arrays.

3. Structural control of ultralong CNTs

Controlling the synthesis of ultralong CNTs is a difficult task due to its harsh growth conditions. The structural control of CNTs involves regulating their tube diameter, wall number, defect density, length, orientation, and array density.[88] The initial step in preparing high-quality CNTs is to control the structural defects caused during growth. These defects, such as vacancies and doping, can significantly impact the properties of CNTs. It has been established through theoretical studies and experimental results that the presence of topological defects in CNTs can lead to a major reduction in their tensile strength by up to 50%.[89] Moreover, the array density of CNTs has high demands for practical applications. For example, the International Business Machines Corporation (IBM) has proposed that the array density of CNTs utilized in integrated circuits should be 125 μm^{-1} (125 000 mm^{-1}).[90] However, traditional methods of preparing ultralong CNTs usually result in an array density of no more than 50 mm^{-1}, making practical application impossible.[7] Hence, it is crucial to develop an effective and feasible method to prepare ultralong CNTs while controlling their structure.

3.1. Control of the length of ultralong CNTs

CNTs can be regarded as one-dimensional linear polymers composed of carbon atoms.[91] The growth process of CNTs is similar to the formation of carbon atom chains. Catalyst particles adsorb and dissolve carbon atoms to create the active center, which initiates the increase of carbon atom chains. The reaction probability of carbon atoms in a discrete state is assumed to be the same for the entire reaction system.[84] This assumption is consistent with the tip-growth mode of CNTs. Therefore, the growth process of CNTs can be seen as a process of carbon atom chain growth with equal probability, which is a kinetically controlled process.

To increase the length of CNTs, a feasible method is to increase the catalytic activity of the catalyst as much as possible while ensuring a sufficient carbon source. Li *et al.* used iron and molybdenum as catalysts to prevent the polymerization of the catalysts with the CNT films extracted from spinnable arrays (Fig. 6a–c).[86] They successfully prepared single-walled CNTs with a length of 18.5 cm. However, if the temperature exceeds the suitable growth temperature range of CNTs, the catalytic activity of the catalyst will increase, which in turn accelerates the cracking of the carbon source. Too much decomposed carbon source will generate amorphous carbon on the surface of the catalyst, which will reduce the activity of the catalyst. Therefore, it is crucial to maintain a constant temperature environment to ensure the activity of the catalyst. However, the tube furnace used for growing CNTs has only a limited constant temperature region, which is not favorable for the synthesis of ultralong CNTs. Wei *et al.* designed a "furnace-moving" method to prepare ultralong CNTs. They successfully obtained ultralong CNTs with lengths of 20 cm and 55 cm by adjusting the growth temperature, water vapor amount, gas velocity, and other parameters (Fig. 6d–j).[82,84] Moreover, the ultralong CNTs have a perfect structure and excellent mechanical properties (Fig. 6k and l).

3.2. Control of the areal density of ultralong CNTs

The high-yield synthesis of ultralong CNTs is a prerequisite for their wide application.[92] However, the low catalyst utilization and aggregation of catalyst particles during the growth process severely limit their yields. In recent years, researchers have developed strategies to improve the density of ultralong CNTs. These methods involve optimizing the catalyst and controlling the growth conditions, such as nanomaterial pinning and rolling, catalyst pre-deposition and multiple growths, and substrate-interception-guided strategies.

3.2.1. Enhancing array density using catalyst/substrate forces. Increasing the areal density of ultralong CNTs can be achieved by inhibiting the aggregation phenomenon of catalysts at high temperatures. Wei *et al.* successfully prevented the aggregation behavior of catalyst particles by introducing silica in the catalyst region (Fig. 7a).[93] They loaded silicon dioxide nanoparticles on the surface of silicon wafers by spin-coating and then annealed them at a certain temperature to remove the residual polymer. Afterward, they coated the wafers with a 0.03 mol L^{-1} $FeCl_3$ solution to use as a catalyst. The presence of silica nanoparticles effectively inhibited the aggregation of the catalyst particles, leading to a significant increase in the density of the horizontal array of CNTs. Another effective method to increase the density of the CNTs horizontal arrays is to use the graphene layer to inhibit the aggregation of catalyst particles (Fig. 7b).[94] The graphene layer was prepared by the CVD method and transferred to the surface of the silicon wafer by etching copper foil with $FeCl_3$ solution. The metal ions remaining on the graphene were reduced to nanoparticles at high temperatures to be used as the catalyst of CNTs. This method effectively suppressed the aggregation behavior of the catalyst and was more efficient than the direct spin-coating of $FeCl_3$ solution for the preparation of CNTs. In this study, the

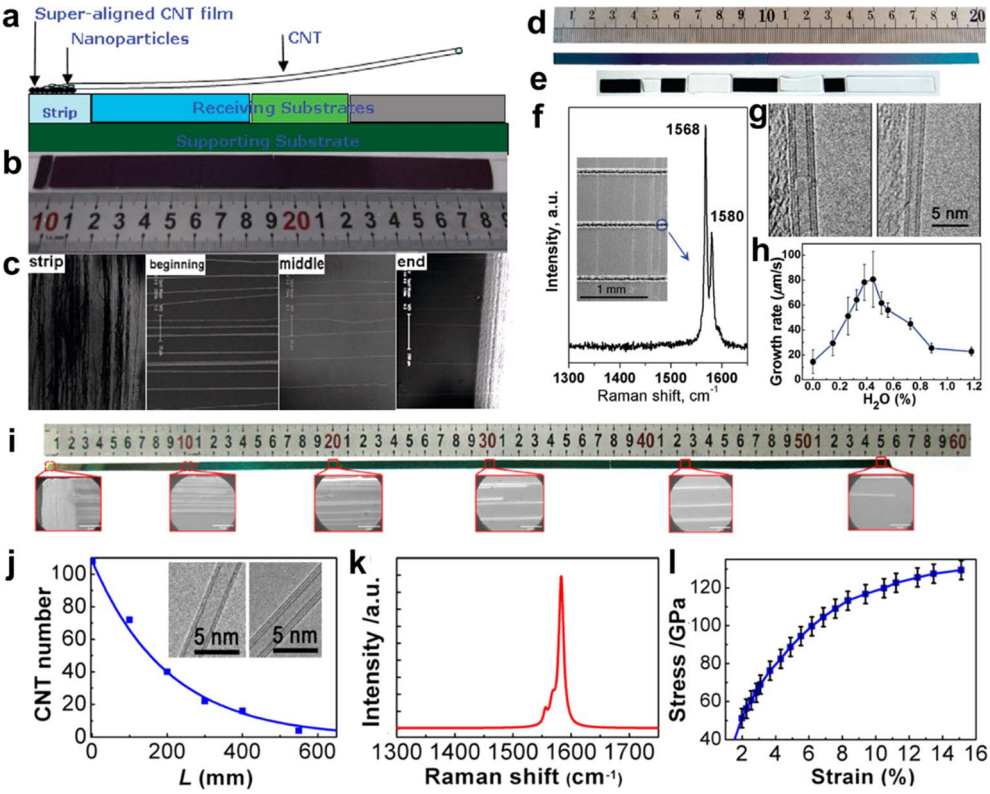

Fig. 6 (a) Schematic of the growth method of the 18.5 cm long CNTs. (b) The optical images of an ultralong CNT array. (c) The SEM images of the strip and the beginning, middle, and end of the ultralong CNT array from left to right.[86] Reproduced from ref. 86 with permission from American Chemical Society, copyright 2009. (d) Optical picture of the 20 cm long Si substrate. (e) Optical picture of the substrate connected by Si (dark substrates) and SiO_2 (white substrates) substrates. (f) Raman spectra and (g) TEM pictures of CNTs. (h) Effect of water concentration on the growth rate of CNTs.[82] Reproduced from ref. 82 with permission from American Chemical Society, copyright 2010. (i) SEM image of the 550 mm long CNTs. (j) Number of CNTs at different lengths on the substrate. Inset: TEM images of as-grown CNTs. (k) Raman spectrum of as-grown CNTs. (l) Mechanical properties of as-grown CNTs.[84] Reproduced from ref. 84 with permission from American Chemical Society, copyright 2013.

wrinkles of graphene also played a pinning role for the catalyst nanoparticles, which limited their movement at high temperatures, thus forming highly dispersed nanoparticles in the catalyst region. The array density obtained by the graphene-assisted growth method was approximately two times higher compared to the conventional microcontact printing method.

The two methods mentioned above utilize the pinning effect of nanomaterials to improve the dispersion of catalyst nanoparticles, which in turn inhibits the aggregation of particles at high temperatures. However, these methods have not been able to address the issue of low catalyst utilization efficiency. Additionally, many short CNTs remain in the catalyst zone, which prevents the intrinsic improvement of ultralong CNTs array density.

3.2.2. Enhancing array density using catalyst pre-deposition and multiple growth. Horizontal arrays of CNTs are usually synthesized by depositing a catalyst on the substrate surface using methods such as drop-coating, spin-coating, micro-contact transfer, and sputtering. However, these catalysts can be random and may aggregate, which can reduce array density and stability in the growth process of ultralong CNTs. To improve the density of the CNT array and the stability of the growth process, Wei *et al.* developed a method where the catalyst is pre-deposited in quartz tubes (Fig. 7c).[95] The catalyst particles are slowly released and transferred to the surface of the substrate during the growth process of CNTs. A catalyst precursor is pre-deposited in the quartz tube at high temperatures, and the catalyst particles deposited in the tube will migrate to the substrate surface of the wafer during the growth of CNTs, particularly at the edge region of the wafer. This *in situ* catalyst pre-deposition strategy allows for multiple reproducible growths with only one loading process, making it possible to grow ultralong CNTs multiple times on the same substrate (Fig. 7d).[95] In this work, the density of ultralong CNT arrays was increased linearly by three repetitive growths, reaching about 54 CNTs per millimeter. This method is highly controllable and reproducible, and it effectively increases the density of horizontal arrays of CNTs.

3.2.3. Enhancing array density using substrate interception and direction strategy (SIDS). The research progress described above focuses on optimizing the growth method of ultralong CNTs by inhibiting the aggregation of catalyst particles. However, the problem of inefficient catalyst utilization remains unsolved. To address this problem, Zhang *et al.* compared the growth mechanisms of floating catalytic chemical vapor deposition (FCCVD) and ultralong CNTs.[31] In the FCCVD

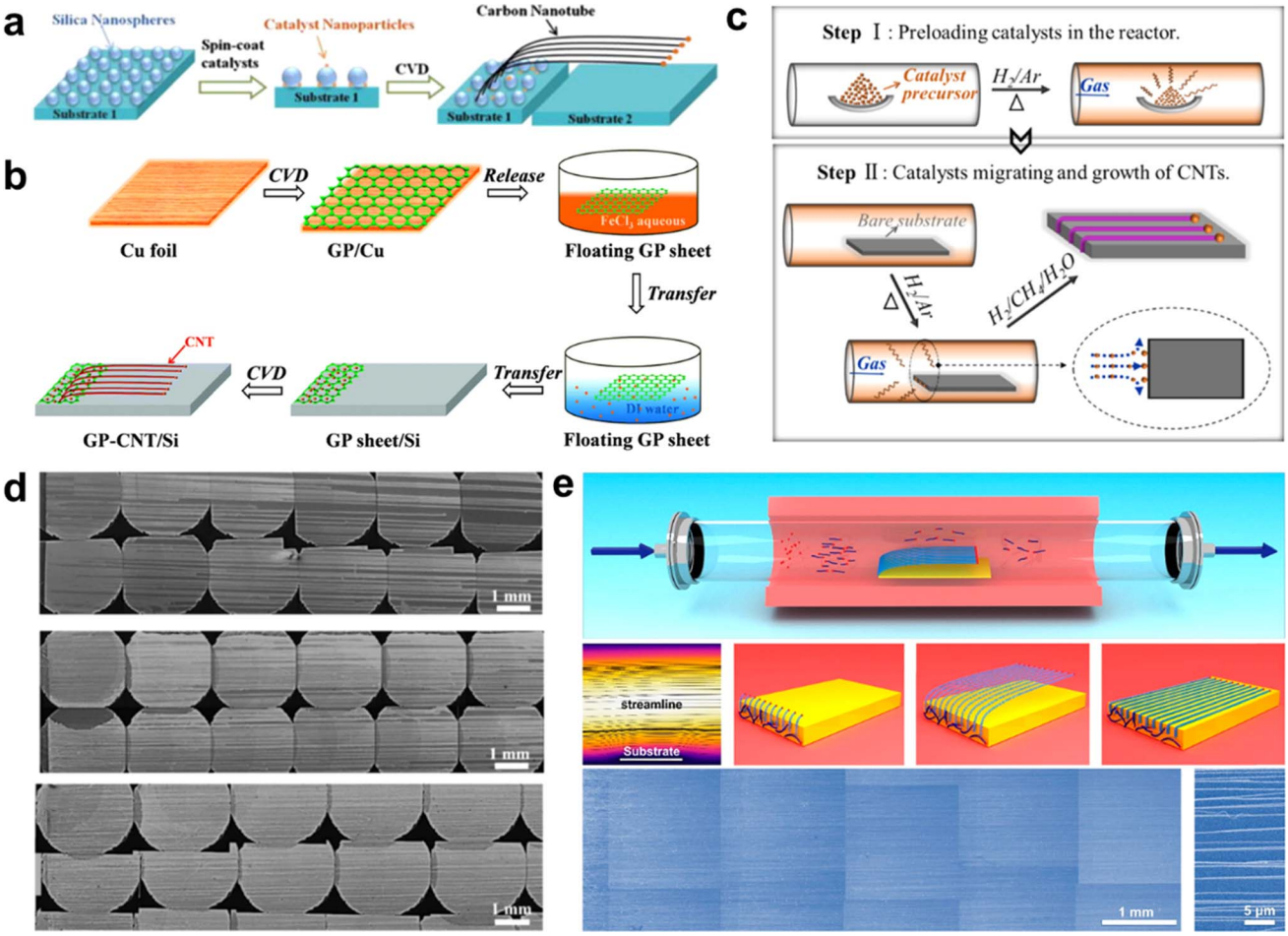

Fig. 7 (a) Inhibition of catalyst particle aggregation and growth of high-density CNT horizontal arrays by silicon dioxide nanospheres.[93] Reproduced from ref. 93 with permission from Elsevier Ltd., copyright 2013. (b) Graphene layer-loaded catalyst particles for growing horizontal arrays of CNTs.[94] Reproduced from ref. 94 with permission from Royal Society of Chemistry, copyright 2014. (c) Schematic diagram of catalyst pre-deposition process. (d) SEM image of multiple growth of ultralong CNTs using a single-deposited catalyst.[95] Reproduced from ref. 95 with permission from Elsevier Ltd., copyright 2016. (e) Synthesis of high-density ultralong CNT arrays by SIDS method.[31] Reproduced from ref. 31 with permission from American Chemical Society, copyright 2023.

process, the catalyst precursor is sublimated and brought into the reactor with a carrier gas, where it undergoes decomposition, reduction, and aggregation at high temperatures to form highly dispersed catalyst nanoparticles. These nanoparticles assist in growing CNTs that float in the gas phase and exit the reactor with the carrier gas.[96] The growth process of FCCVD is similar to that of ultralong CNTs, as both results in CNTs that float in the gas phase and have high quality and low wall counts.[97] However, there are differences in growth processes. In FCCVD, the CNTs do not attach to a substrate, so their growth time is short. In contrast, one end of ultralong CNTs is fixed to a substrate, allowing for longer growth times of up to several hours. By fixing one end of CNTs grown through FCCVD to a substrate, it is possible to prolong their growth time and convert them into ultralong CNTs, thereby enhancing the preparation efficiency of ultralong CNTs.

Zhang *et al.* proposed a SIDS way to achieve high-yield preparation of ultralong CNTs (Fig. 7e).[31] In this study, short CNTs in the gas phase were intercepted by a flat substrate placed inside the FCCVD device. The substrate edge splits the gas flow, immobilizing one end of the CNTs. Then, the CNTs floated up under the guidance of the gas flow and the lifting effect of the thermal buoyancy force, continuously growing into ultralong CNTs. This method efficiently couples FCCVD with the growth process of ultralong CNTs, resulting in a significant increase in the utilization efficiency of the catalyst. Additionally, the aggregation of catalyst nanoparticles was effectively suppressed, which led to a significant increase in the yield of ultralong CNTs. The researchers successfully produced ultralong CNTs with the highest array density of 6700 nanotubes per mm, which is 2–3 orders of magnitude higher than that of the conventional method. Moreover, the ultralong CNTs prepared by SIDS can reach lengths on the order of decimeters, with uniform and continuous morphology and high orientation. The TEM test shows that the ultralong CNTs have high crystallinity, clean surfaces, and low wall counts, confirming that the ultralong CNTs have very high crystallinity.

3.3. Control of the wall number and diameter of ultralong CNTs

The length index of ultralong CNTs is critical, but their structural control is equally important.[7] This control includes ensuring the structural consistency of CNTs, controlling the number of tube walls, managing the diameter, and selecting the chirality. Among these factors, controlling the wall number and diameter of CNTs is achievable by changing the catalyst particle type, adjusting the catalyst size, regulating the growth temperature, altering the raw materials, and other similar methods.[98–100]

3.3.1. Catalyst-determined wall number and diameter control. The growth of CNTs greatly depends on the presence of a catalyst. The size and types of catalyst particles play a crucial role in determining the diameter and number of walls in CNTs.[36,101] Different catalysts have different properties and cause various aggregation behaviors at different temperatures, which affect the size of catalyst particles.[102] It has been observed that larger catalyst particles lead to larger tube diameters in CNTs.[103] As a result, it is possible to prepare horizontal arrays of CNTs with selective tube diameters by controlling the type, size, and dispersion of the catalyst particles.

Metal catalysts, such as iron, copper, and cobalt, are commonly used for the preparation of ultralong CNTs. Iron and copper catalysts are preferred due to their lower melting and boiling points, as well as weaker forces with silicon substrates, which make it easier to catalyze the growth of horizontal arrays of CNTs.[104] Experiments and molecular dynamics simulations have shown that adjusting the surface energy of copper particles results in smaller and more uniformly distributed particles, leading to a smaller and more concentrated tube diameter distribution of CNTs formed from copper catalysts. Moreover, catalyst particle sizes can be controlled by adjusting the concentration of the catalyst precursor, allowing for selective distribution of tube diameters in horizontal arrays of CNTs. Hong *et al.* used different concentrations of $FeCl_3$ solutions as the catalyst precursor to prepare horizontal arrays of single-walled CNTs (SWCNT) and multi-walled CNTs (MWCNT).[105]

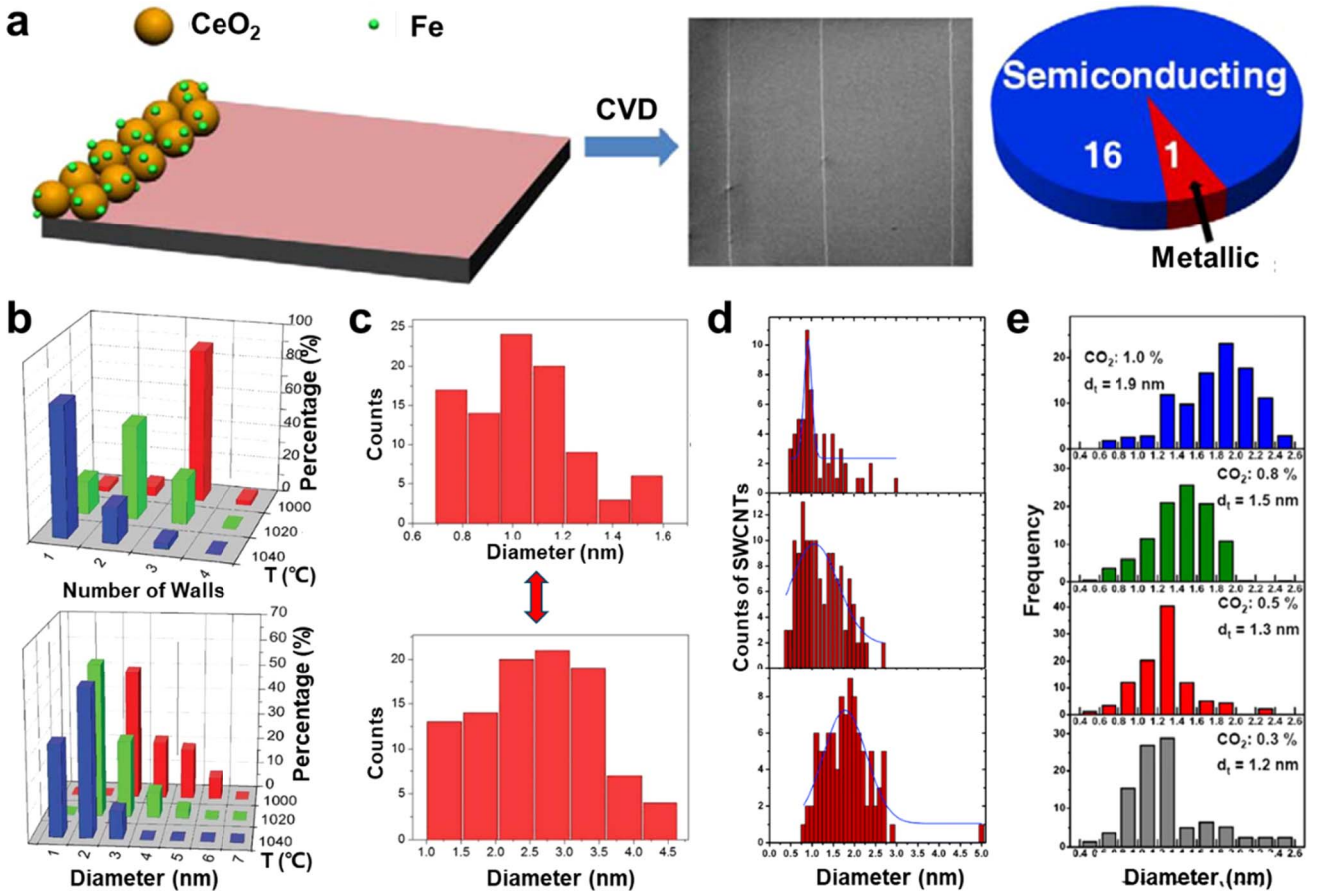

Fig. 8 (a) Cerium oxide as a catalyst particle carrier for the preparation of highly selective semiconductor-type CNT horizontal arrays.[106] Reproduced from ref. 106 with permission from American Chemical Society, copyright 2014. (b) Effect of temperature on wall number and diameter of CNTs.[107] Reproduced from ref. 107 with permission from Wiley-VCH, copyright 2010. (c) Different carbon sources (up: CO gas, down: CH_4 gas) lead to the growth of SWCNTs with different diameter distributions.[108] Reproduced from ref. 108 with permission from Royal Society of Chemistry, copyright 2012. (d) Diameter distributions of SWCNTs grown at different ethane concentrations at 900 °C (up to down: 140 ppm, 1600 ppm, and 14 400 ppm, respectively).[109] Reproduced from ref. 109 with permission from American Chemical Society, copyright 2006. (e) The fitted diameter diagrams of the SWCNT samples as a function of CO_2 concentration.[110] Reproduced from ref. 110 with permission from Elsevier Ltd., copyright 2011.

However, catalyst particles tend to aggregate at high temperatures, so carrier materials are used to disperse the catalyst particles and reduce aggregation. Jiang *et al.* synthesized SWCNT horizontal arrays with a uniform diameter distribution by using a single layer of spinnable CNTs as the catalyst carrier, which prevented catalyst aggregation. The electrical properties of these CNTs were homogeneous and consistent over a length range. Additionally, oxide materials have been used as catalyst carriers. Li *et al.* used cerium oxide (CeO_2) loaded with iron or cobalt nanoparticles to prepare semiconducting SWCNT horizontal arrays (Fig. 8a).[106] CeO_2 is stable at high temperatures and has an oxygen storage capacity, which allows for the etching of metal-type CNTs, resulting in highly selective semiconducting CNT arrays. CNTs created using this method have a narrow tube size distribution, and the proportion of semiconductor-type CNTs can reach over 93%.

3.3.2. Temperature-determined wall number and diameter control. The number of walls and diameter of ultralong CNTs can be controlled by regulating the growth conditions of CNTs, mainly by controlling the growth temperature. Wei *et al.* discovered that the temperature has a direct relationship with the wall numbers of ultralong CNTs during the preparation of CNTs horizontal arrays using the air-flow induced method (Fig. 8b).[107] As the growth temperature increases, the wall number and diameter of CNTs decrease. At a growth temperature of 1000 °C, the proportion of three-walled CNTs reaches 90%. At 1020 °C, the percentage of double-walled CNTs increases to more than 50%, and the three-walled CNTs decrease to about 20%. With further temperature increases, the proportion of SWCNT can reach up to 70%, and the three-walled CNTs account for less than 10%. Moreover, the CNTs produced by this method are characterized by structural consistency in the macroscopic length range (>60 mm), as noted by the researchers.

Zhang *et al.* researched the effect of temperature on the diameter of CNTs.[111] They discovered that by changing the growth temperature during the process, it is possible to create intramolecular junctions between CNTs of different diameters. This work confirmed that the diameter of CNTs can be reduced by increasing the reaction temperature during growth. This happens because the carbon-solubilizing capacity of catalyst particles changes after the temperature increases, which affects their shape. The temperature change also impacts the interaction between CNTs and catalysts. Furthermore, increasing the temperature reduces the stiffness of the carbon layer, which makes it more favorable for the growth of small-diameter CNTs with high-strain energy.

3.3.3. Feedstock-determined wall number and diameter control. It has been found that feedstock is a crucial factor that affects catalyst activity. Researchers usually use methane or ethanol as a carbon source in growing ultralong CNTs. Many studies have shown that adding a small amount of water can greatly improve the growth of ultralong CNTs during the CVD growth process.[82] The concentration of water is a key factor affecting catalyst activity. The H_2/CH_4 ratio is also important in the chemical equilibrium of CNT growth and affects catalyst activity. Additionally, the growth of ultralong CNTs is promoted by adding CO gas. For example, He *et al.* discovered that Fe nanoparticles on TEM grids catalyzed the growth of CNTs using CO as a carbon source, producing SWCNTs with diameters ranging from 0.7 to 16 nm. They found that different carbon sources produced CNTs with varying chiral angles (Fig. 8c).[108] Moreover, H_2 gas is crucial in the nucleation of large-diameter SWCNTs. Liu *et al.* found that the diameter distribution of CNTs can be controlled by selective activation of nanoparticles during the growth phase (Fig. 8d).[109] They demonstrated that even highly dispersed nanoparticles can be used as catalysts to control the diameter of SWCNTs. Nasibulin *et al.* proposed a method to adjust the diameter of SWCNTs in the range of 1.1 to 1.9 nm by controlling the growth conditions in the reactor (Fig. 8e).[110] Kauppinen *et al.* discovered that the addition of CO_2 to CO can effectively control the nucleation of SWCNTs with a certain average diameter.[112] They concluded that CO_2 acts as an etchant to selectively etch small-diameter tubes.

3.4. Control of the morphology of ultralong CNTs

By altering the reactor configuration and reaction conditions, ultralong CNTs with different structures such as crossed CNT networks, CNT forests, and suspended CNT structures can be obtained.[113,114] It is also necessary to adjust their morphology in a controllable way, except for the length, density, and diameter to meet their applications.

3.4.1. Synthesis of ultralong CNTs bundles (CNTBs). CNTs have a lot of potential to produce super-strong fibers.[115] However, when conventional short CNTs are used, the strength of the fibers is negatively impacted by various factors such as defects, impurities, irregular orientation, discontinuous structure, and length. The reported strength of CNT fibers is usually only 0.5 to 11.5 GPa, which is significantly lower than the theoretical strength, which is greater than 100 GPa. The issue is primarily because the average length of the CNTs used to make the fibers is relatively short, and the units are lapped to each other with van der Waals forces. This makes it easy for them to slip under tensile force, and the intrinsic high strength of CNTs cannot be fully harnessed. Additionally, structural defects and disordered orientations within CNTs can also contribute to a decrease in fiber strength. On the other hand, ultralong CNTs have many advantages in the production of super-strong fibers, including their length of up to centimeters or even decimeters, perfect structures, consistent orientation, and mechanical properties that are close to the theoretical limit.

Wei *et al.* have successfully developed a method to prepare long and continuous CNTBs that have a consistent structure and orientation (Fig. 9a–c).[78] By using a gas-flow focusing technique, they were able to produce CNTBs of varying lengths and compositions. The researchers studied the mechanical properties of these CNTBs and found that the overall strength of the bundles was influenced by the "Daniel effect". They discovered that the tensile strength of CNTBs can be increased to over 80 GPa by relaxing the initial stress of the CNTs using a "simultaneous relaxation and tension" strategy. This approach allowed the tensile strength of a bundle containing an unlimited number of ultralong CNTs to be close to that of

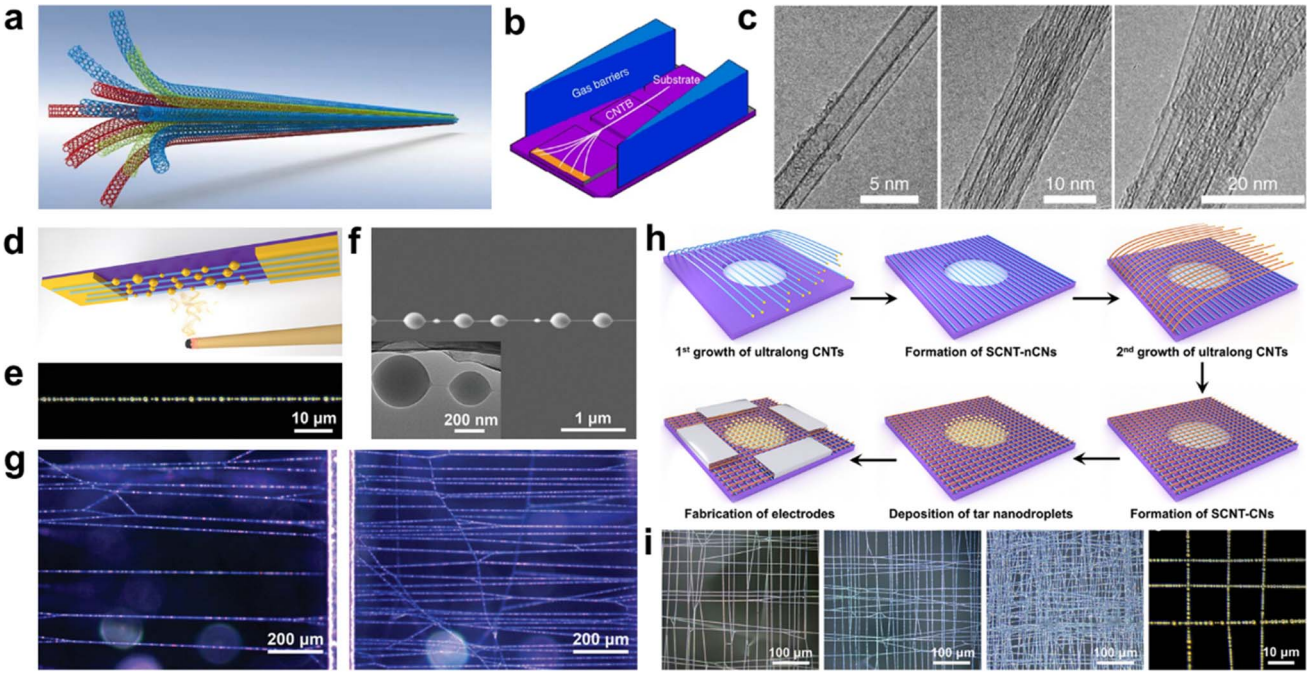

Fig. 9 (a) Schematic illustration of ultralong CNTBs composed of continuous CNTs. (b) Schematic illustration of the *in situ* fabrication of CNTBs by the gas-flow focusing method. (c) TEM images of CNTBs with different component numbers.[78] Reproduced from ref. 78 with permission from Springer Nature, copyright 2018. (d) Optical visualization diagram, (e) optical picture, and (f) SEM picture of a single SCNTN. (g) Optical microscopy images of SCNTNs with different areal densities.[114] Reproduced from ref. 114 with permission from Wiley-VCH, copyright 2022. (h) Synthesis and (i) morphologies of SCNT-CNs.[33] Reproduced from ref. 33 with permission from American Chemical Society, copyright 2024.

a single nanotube, if the bundle was of continuous length, had a perfect structure and consistent orientation, and the initial stress was uniformly distributed. The promising findings of this study suggest that ultralong CNTs could be used to create super-strong fibers and provide a direction and methodology for the development of new types of super-strong fibers.[17]

3.4.2. Synthesis of suspended ultralong CNTs. Suspended nanostructures have a large specific surface area, which benefits the adsorption and mass transfer of small molecules.[116] Recently, suspended CNTs have found extensive use in the preparation of high-performance optoelectronic devices, sensors, and other such applications.[117,118] Zhang *et al.* achieved controllable preparation of suspended CNT networks (SCNTNs) using the SIDS method mentioned earlier (Fig. 9d–g).[114] Ultralong CNTs following a floating growth mode can form overhanging structures across the grooves on the surface of the silicon substrate. Due to the lack of substrate confinement at the overhangs, the suspended high-density ultralong CNTs self-assemble under van der Waals forces to form SCNTNs. After growth, the SCNTNs can be uniformly loaded with tar nanodroplets for optical visualization using a smoke-assisted rapid *in situ* optical visualization technique. As illustrated in Fig. 9h and i, the group proposed a strategy for constructing suspended carbon nanotube-crossed networks (SCNT-CN).[33] A square silicon wafer with circular holes was used as a growth substrate. First, a unidirectional SCNTN structure was grown using SIDS. Next, the substrate was rotated by 90° and then grown a second time. The SCNT-CN can be spontaneously assembled by lapping the suspended CNTs under van der Waals forces. The cross-lattice structure of suspended CNTs with different surface densities can be obtained by adjusting the growth time.

4. Properties and applications of ultralong CNTs

The unique structures, huge aspect ratios, defect-free structures, and macroscopic lengths endow the ultralong CNTs with excellent properties and novel characteristics. Many studies have been conducted on the properties of ultralong CNTs which exhibited superior mechanical, electrical, and thermal performance.

4.1. Extraordinary properties of ultralong CNTs

Ultralong CNTs possess remarkable mechanical properties including tensile strength above 100 GPa, Young's modulus above 1 TPa, and elongation at break of more than 17% (Fig. 10a and b).[78] The ultralong CNTs exhibit a superior fatigue resistance, with the ability to withstand large-strain cyclic tensile tests without breaking (Fig. 10c and d).[80] Furthermore, ultralong CNTs display high mobility and consistency in their electrical properties, as discovered by Fan *et al.*,[86] and wide linear intervals of up to 120 dB in photodiodes, as observed by Peng *et al.*[120] In terms of thermal properties, an extremely high heat transfer coefficient of approximately 8.9×10^4 Wm^{-2} K^{-1} between a single suspended ultralong CNTs and air was also reported.[79] Besides, Wei *et al.* also found the superlubrication in the centimeter-length CNTs in an

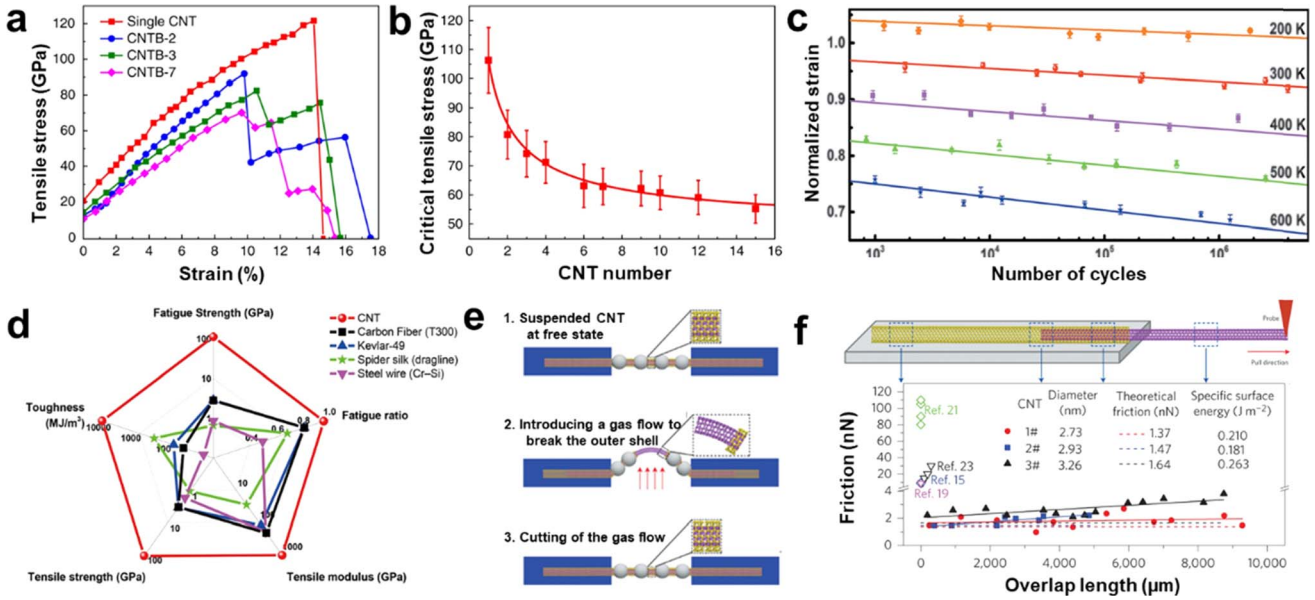

Fig. 10 (a) Stress–strain curves for single CNTs and CNTBs with gauge lengths of about 1.5 mm. (b) The relationship between the tensile strength of CNTBs and the CNTB component numbers.[78] Reproduced from ref. 78 with permission from Springer Nature, copyright 2018. (c) Fatigue behavior of CNTs at different temperatures. (d) Comparison of mechanical performance between CNTs and some high-performance materials.[80] Reproduced from ref. 80 with permission from American Association for the Advancement of Science, copyright 2020. (e) Illustrations showing inner-shell sliding processes for ultralong DWCNTs. (f) Schematic of an inner shell being pulled out of a DWCNT and intershell friction of three DWCNTs with different outer diameters.[119] Reproduced from ref. 119 with permission from Springer Nature, copyright 2013.

atmospheric environment (Fig. 10e and f).[119] The superlubrication scale was three orders of magnitude higher than the highest value reported before. The friction between CNT layers was measured to be as low as 1–2 nN, which is 5–100 times better than previous experimental results. The shear strength obtained is 4 orders of magnitude lower than the lowest value of literature results and is independent of the length of the contact. This means that ultralong CNTs have the potential to provide a new material platform and perspective to study unique surface-interface phenomena at the nanoscale.

4.2. Applications of ultralong CNTs

Ultralong CNTs are promising candidates for high-performance field-effect transistors (FETs). Ultralong CNTs have carrier mobility as high as 10^5 cm^2 V^{-1} s^{-1} and an ultra-high saturation speed. Furthermore, CNTs can form ohmic contacts with specific metal electrodes to achieve ballistic transport, and are compatible with low-temperature semiconductor manufacturing processes, making them suitable for the construction of large-scale integrated circuits. Wei *et al.* synthesized high-density ultralong CNT arrays up to 65 cm long on multiple 4-inch wafers by utilizing catalyst pre-deposition and multiple growths (Fig. 11a).[79] They constructed large-scale FET devices on these ultralong CNT arrays to characterize their electrical properties. The results showed that most of the FET devices exhibit high open-state currents, high switching ratios, and high mobility (Fig. 11b). Additionally, they introduced a certain frequency of acoustic waves during the growth of ultralong CNTs, which enabled the self-assembly of CNTs into CNT wire clusters. The obtained CNT assemblies have high open-state currents, which satisfy the application of CNTs in nanodevices. Zhang *et al.* successfully fabricated decimeter-scale ultralong CNTs with an array density of 6700 CNTs/mm using the SIDS method and produced large-scale arrays of FET devices.[31] This work found that the switching ratio of the FET devices was generally elevated with the increase of the array length. In addition, the open-state current of the FET decreases slowly with the increase of the array length. These results indicated that the array density of ultralong CNTs decays gradually with the increase of the length, which is in good agreement with the Schulz–Flory distribution law of ultralong CNTs. This work takes advantage of the spontaneous purification behavior of ultralong CNTs to measure FET composed of pure semiconductor-type CNTs with switching ratios as high as 4.2×10^5. All in all, these results demonstrate the potential of ultralong CNTs for application in high-performance FET devices.

CNTs are materials that have a direct bandgap and high absorption coefficients in a wide range of spectral frequencies, from ultraviolet to terahertz bands. The intrinsic response time of CNTs is very fast, on the order of 10^{-12} seconds. These properties make CNTs potentially useful for high-performance photodetectors, and they are expected to outperform conventional photodetector materials like InGaAs and HgCdTe under room-temperature operating conditions.[122] However, there have been few studies on ultralong CNTs due to difficulties in preparing them efficiently. One study by Peng and Wang involved constructing Pd–Sc asymmetric fork-finger electrodes on a single ultralong CNT to create a diode-configured photodetector.[122] The researchers found that when the laser power

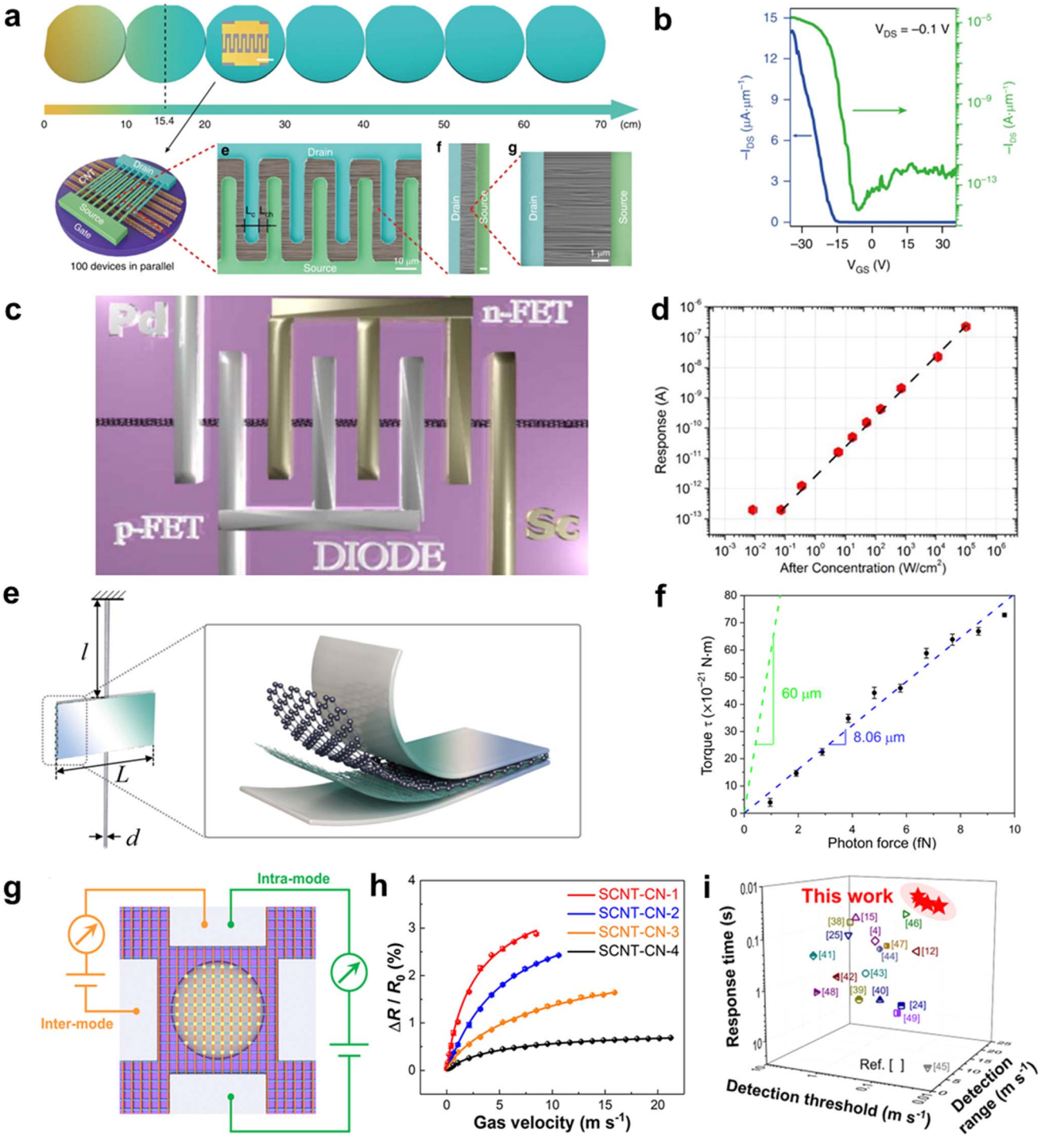

Fig. 11 (a) FET devices based on ultralong CNT arrays. (b) Transfer characteristics of the width normalized transistor for a single channel plotted in both linear (blue, left axis) and logarithmic (green, right axis) scales with applied V_{DS} of −0.1 V.[79] Reproduced from ref. 79 with permission from Springer Nature, copyright 2019. (c) A 3D sketch of the device for high-frequency measurement. (d) The high-frequency response of the photodetector at 0 V.[120] Reproduced from ref. 120 with permission from AIP Publishing LLC, copyright 2014. (e) Schematic illustration of the torsion balance unit. (f) Torque *versus* incident photon force.[121] Reproduced from ref. 121 with permission from American Association for the Advancement of Science, copyright 2021. (g) Schematic illustration of the inter and intramode for the testing of SCNT-CNs-based airflow sensors. (h) Relative resistance variation of SCNT-CNs with different areal densities under different gas velocities. (i) Performance comparison between SCNT-CNs-based airflow sensors and previously reported airflow sensors.[33] Reproduced from ref. 33 with permission from American Chemical Society, copyright 2024.

density ranged from 10^{-1} to 10^{5} W cm^{-2}, the response current of the device at zero bias showed perfect linear behavior, corresponding to a linear interval of 120 dB (Fig. 11c and d).[120] The photocurrent reached up to 545.65 nA at 10^{5} W cm^{-2} power density and optimal polarization. The authors attributed the wide linear interval to the ultralong CNT's high mobility, short channel length, high charge collection efficiency, and non-doped device preparation process.

Ultralong CNTs possess a high aspect ratio, high flexibility, and high modulus, which makes them highly responsive to external fields. When designed as suspended devices, they can be used to create mechanical sensors with high sensitivity. Jiang *et al.* recently developed a sandwich-structured torsion scale by utilizing the large aspect ratio and flexibility of ultralong CNTs (Fig. 11e and f).[121] The scale consists of an aluminum membrane, a graphene-CNT membrane, and ultralong CNTs. A low-power laser was focused and irradiated onto the torsion scale, and even a weak light pressure could cause it to twist. The angle of torsion was measured by determining the displacement of the spot after the laser light was reflected by the aluminum membrane. The torsion scale can measure forces as low as 10^{-15} N with a torsional spring constant of only 8.72×10^{-18} N m rad^{-1} and a sensitivity of about 10^{13} rad N^{-1}. This superior performance makes it an ideal option when compared to other materials.

Airflow sensors have very important applications in aerospace, weather forecasting, environmental monitoring, the chemical industry, biomedicine, health monitoring, and smart wearable devices.[123] However, traditional airflow sensors have limitations such as slow response rate, low sensitivity, high detection limit, narrow detection range, and large hysteresis.[124] These limitations hinder the sensor's applications in various fields. CNTs possess excellent mechanical and electrical properties, making them an ideal candidate for airflow sensors.[114] However, in most current reports on airflow sensors, CNTs are usually combined with rigid matrix materials, which greatly limits their displacement and deformation under airflow trailing forces. This leads to poor sensitivity and response speed of the devices. Additionally, the reports often use multi-walled CNTs containing more defects, which further degrades the device's performance. Zhang *et al.* developed a high-performance airflow sensor using SCNTNs (Fig. 11g–i).[33] They modified the nanoparticles on the surface of CNTs networks to achieve optical visualization, structural stability, and enhancement of airflow traction. The ultralight and extremely flexible structure of the ultralong SCNTN gave it superior sensing performance than most airflow sensors. The airflow sensor showed a very short response time (0.021 s), high sensitivity (0.0124 sm^{-1}), low detection threshold (0.02 ms^{-1}), and wide detection range (0.02–21 ms^{-1}). The comprehensive performance of this sensor is significantly better than most current reports.

5. Summary and outlook

In this review, we discussed the growth mechanism, controlled synthesis, properties, and applications of ultralong CNTs. Ultralong CNTs have been widely investigated in recent years due to their perfect structures and excellent properties, while challenges remain, *i.e.*, the structure-controlled synthesis and mass preparation of high-quality ultralong CNTs without structural defects. However, these challenges are also accompanied by potential opportunities for ultralong CNTs to be applied in more cutting-edge fields. Ultralong CNTs are preferred for preparing super-strong CNT fibers. Except for low defects, increasing the yield and reducing the cost are the keys to achieving the large-scale application of ultra-strong CNT fibers. Ensuring high performance while avoiding over-treatment is also important to be considered for producing super-strong and high-performance CNT fibers. Herein, we propose the following outlooks for the field of ultralong CNTs.

Firstly, novel theoretical and experimental techniques are expected to be incorporated into studying growth mechanisms and synthetic methodologies. For example, deeper understandings of the growth mechanisms of ultralong CNTs may be anticipated using artificial intelligence (AI) and multiscale theoretical simulations. AI-assisted research may unveil the key factors hidden behind the growth behavior of ultralong CNTs, which can hardly be resolved under traditional research paradigms. Moreover, combining the electronic structures revealed by *ab initio* simulations, atomic and molecular structures revealed by molecular dynamics, and macroscale structures revealed by computational fluid dynamics, a complete vision of the growth mechanisms containing multiple spatiotemporal scales is expected to be established. In the aspects of experimental techniques, *in situ* characterization techniques may enable the collection of abundant information during the growth of ultralong CNTs. *In situ* Raman spectroscopy, TEM, and SEM characterizations can be combined with reactors to demonstrate the dynamic changes of multiple physical fields, establish the correlations between growth conditions and CNT structures, and facilitate the optimization of experimental protocols. Secondly, advanced techniques for the mass production of ultralong CNTs should be developed. The coupled processes of momentum transfer, heat transfer, mass transfer, and reactions are expected to be thoroughly investigated both in computational and experimental manners. Based on the fundamental growth mechanisms and scale-up principles, reactors with higher capabilities should be rationally designed and tested to further increase the yields and uniformity of ultralong CNT products. Finally, functionalization strategies need to be further developed for *in situ* modification or efficient compounding of ultralong CNTs, leading to the design of multi-functional, high-performance devices to fully exploit the ultimate properties of ultralong CNTs.

In summary, more effort is needed in the future. More investigations are required in developing large-scale synthesis techniques, studying special properties, and exploring new applications of ultralong CNTs.

Data availability

No primary research results, software or code have been included and no new data were generated or analysed as part of this review.

Author contributions

Kangkang Wang: conceptualization, writing – original draft, writing – review & editing. Fei Wang: writing – original draft, writing – review & editing. Qinyuan Jiang: writing – review & editing. Ping Zhu: writing – review & editing. Khaixien Leu: writing – review & editing. Rufan Zhang: supervision, project administration, funding acquisition, writing – review & editing. All authors have given approval to the final version of the manuscript.

Conflicts of interest

There are no conflicts to declare.

Acknowledgements

This work is supported by the National Key Research and Development Program (Grant No. 2020YFC2201103 and 2020YFA0210702) and National Natural Science Foundation of China (Grant No. 51872156 and 22075163).

References

1 T. O. Wehling, A. M. Black-Schaffer and A. V. Balatsky, *Adv. Phys.*, 2014, **63**, 1–76.
2 S. Ghosh, S. Barg, S. M. Jeong and K. K. Ostrikov, *Adv. Energy Mater.*, 2020, **10**, 2001239.
3 K. D. Patel, R. K. Singh and H.-W. Kim, *Mater. Horiz.*, 2019, **6**, 434–469.
4 D.-M. Sun, M. Y. Timmermans, A. Kaskela, A. G. Nasibulin, S. Kishimoto, T. Mizutani, E. I. Kauppinen and Y. Ohno, *Nat. Commun.*, 2013, **4**, 2302.
5 S. Chen, L. Qiu and H.-M. Cheng, *Chem. Rev.*, 2020, **120**, 2811–2878.
6 T. Chen and L. Dai, *J. Mater. Chem. A*, 2014, **2**, 10756–10775.
7 R. Zhang, Y. Zhang and F. Wei, *Chem. Soc. Rev.*, 2017, **46**, 3661–3715.
8 R. Li, Q. Jiang and R. Zhang, *Sci. Bull.*, 2022, **67**, 784–787.
9 R. Zhang, Q. Wen, W. Qian, D. S. Su, Q. Zhang and F. Wei, *Adv. Mater.*, 2011, **23**, 3387–3391.
10 K. Chen, W. Gao, S. Emaminejad, D. Kiriya, H. Ota, H. Y. Y. Nyein, K. Takei and A. Javey, *Adv. Mater.*, 2016, **28**, 4397–4414.
11 Y. Zhan, R. Zhao, Y. Lei, F. Meng, J. Zhong and X. Liu, *Appl. Surf. Sci.*, 2011, **257**, 4524–4528.
12 C. Rutherglen and P. Burke, *Small*, 2009, **5**, 884–906.
13 B. D. Jensen, J.-W. Kim, G. Sauti, K. E. Wise, J. M. Gardner, J. G. Smith, R. A. Wincheski, R. J. Cano and E. J. Siochi, *ACS Appl. Nano Mater.*, 2023, **6**, 9558–9568.
14 D. Yu, K. Goh, H. Wang, L. Wei, W. Jiang, Q. Zhang, L. Dai and Y. Chen, *Nat. Nanotechnol.*, 2014, **9**, 555–562.
15 N. M. Bandaru and N. H. Voelcker, *J. Mater. Chem.*, 2012, **22**, 8748–8758.
16 J. Sun, Z. Zhao, Z. Li, Z. Zhang, R. Zhang and X. Meng, *J. Mater. Chem. A*, 2023, **11**, 22430–22440.
17 R. Zhang, Y. Zhang and F. Wei, *Acc. Chem. Res.*, 2017, **50**, 179–189.
18 N. Saito, Y. Usui, K. Aoki, N. Narita, M. Shimizu, K. Hara, N. Ogiwara, K. Nakamura, N. Ishigaki, H. Kato, S. Taruta and M. Endo, *Chem. Soc. Rev.*, 2009, **38**, 1897–1903.
19 Y. Zhao, R. Li, B. Wang, Y. Huang, P. Lyu, F. Wang, Q. Jiang, Y. Han, S. Zhang, X. Wu, S. Zhao, N. Zhu and R. Zhang, *ACS Nano*, 2023, **17**, 2893–2900.
20 R. Li, S. Zhang, H. Chen, Y. Huang, B. Wang, X. Wu, Q. Jiang, S. Zhao, F. Wang, Y. Zhao and R. Zhang, *SusMat*, 2023, **3**, 102–110.
21 F. Wang, S. Zhao, Q. Jiang, R. Li, Y. Zhao, Y. Huang, X. Wu, B. Wang and R. Zhang, *Cell Rep. Phys. Sci.*, 2022, **3**, 100989.
22 S. Muhl, R. Aguilar Osorio and U. A. Martinez Huitle, *Rev. Mex. Fis.*, 2017, **63**, 439–447.
23 D. Janas, S. Boncel and K. K. K. Koziol, *Carbon*, 2014, **73**, 259–266.
24 Y. Liu and S. Kumar, *ACS Appl. Mater. Interfaces*, 2014, **6**, 6069–6087.
25 J. Si, L. Liu, F. Wang, Z. Zhang and L.-M. Peng, *ACS Nano*, 2016, **10**, 6737–6743.
26 C. Wang, J.-C. Chien, K. Takei, T. Takahashi, J. Nah, A. M. Niknejad and A. Javey, *Nano Lett.*, 2012, **12**, 1527–1533.
27 M. Endo, T. Hayashi and Y.-A. Kim, *Pure Appl. Chem.*, 2006, **78**, 1703–1713.
28 J. Ma, Z. Zhu, B. Chen, M. Yang, H. Zhou, C. Li, F. Yu and J. Chen, *J. Mater. Chem. A*, 2013, **1**, 4662–4666.
29 Q. Ye, A. M. Cassell, H. B. Liu, K. J. Chao, J. Han and M. Meyyappan, *Nano Lett.*, 2004, **4**, 1301–1308.
30 Q. Jiang, F. Wang, R. Li, X. Wu, W. Zhang, S. Zhao, Y. Huang, B. Wang, S. Zhang, Y. Zhao and R. Zhang, *Adv. Funct. Mater.*, 2023, **33**, 2212665.
31 Q. Jiang, F. Wang, R. Li, B. Li, N. Wei, N. Gao, H. Xu, S. Zhao, Y. Huang, B. Wang, W. Zhang, X. Wu, S. Zhang, Y. Zhao, E. Shi and R. Zhang, *Nano Lett.*, 2023, **23**, 523–532.
32 F. Chen, Y. Huang, R. Li, S. Zhang, Q. Jiang, Y. Luo, B. Wang, W. Zhang, X. Wu, F. Wang, P. Lyu, S. Zhao, W. Xu, F. Wei and R. Zhang, *Sci. Adv.*, 2022, **8**, eabn5882.
33 Q. Jiang, K. Leu, X. Gong, F. Wang, R. Li, K. Wang, P. Zhu, Y. Zhao, Y. Zang and R. Zhang, *ACS Appl. Mater. Interfaces*, 2024, **16**, 20949–20958.
34 X. K. Wang, X. W. Lin, V. P. Dravid, J. B. Ketterson and R. P. H. Chang, *Appl. Phys. Lett.*, 1995, **66**, 2430–2432.
35 Y. Wang, Q. Zhang, Z. Liu, R. Huang and L. Zheng, *Acta Phys.-Chim. Sin.*, 1996, **12**, 905–909.
36 K. A. Shah and B. A. Tali, *Mater. Sci. Semicond. Process.*, 2016, **41**, 67–82.
37 J. Robertson, G. Zhong, S. Esconjauregui, C. Zhang, M. Fouquet and S. Hofmann, *Phys. Status Solidi B*, 2012, **249**, 2315–2322.
38 M. Jung, K. Y. Eun, J. K. Lee, Y. J. Baik, K. R. Lee and J. W. Park, *Diamond Relat. Mater.*, 2001, **10**, 1235–1240.
39 I. Stassen, M. Styles, G. Grenci, H. Van Gorp, W. Vanderlinden, S. De Feyter, P. Falcaro, D. De Vos, P. Vereecken and R. Ameloot, *Nat. Mater.*, 2016, **15**, 304–310.

40 B. Liu, L. Chen, G. Liu, A. N. Abbas, M. Fathi and C. Zhou, *ACS Nano*, 2014, **8**, 5304–5314.
41 R. M. Silva, M. C. Ferro, J. R. Araujo, C. A. Achete, G. Cavel, R. F. Silva and N. Pinna, *Langmuir*, 2016, **32**, 7038–7044.
42 F. Beuneu, *Solid State Commun.*, 2005, **136**, 462–465.
43 M. He, H. Amara, H. Jiang, J. Hassinen, C. Bichara, R. H. A. Ras, J. Lehtonen, E. I. Kauppinen and A. Loiseau, *Nanoscale*, 2015, **7**, 20284–20289.
44 F. Ding, K. Bolton and A. Rosén, *J. Phys. Chem. B*, 2004, **108**, 17369–17377.
45 F. Ding, K. Bolton and A. Rosén, *Comput. Mater. Sci.*, 2006, **35**, 243–246.
46 Q. Jin, S. Jiang, Y. Zhao, D. Wang, J. Qiu, D.-M. Tang, J. Tan, D.-M. Sun, P.-X. Hou, X.-Q. Chen, K. Tai, N. Gao, C. Liu, H.-M. Cheng and X. Jiang, *Nat. Mater.*, 2019, **18**, 62–68.
47 Y. Ohta, Y. Okamoto, S. Irle and K. Morokuma, *ACS Nano*, 2008, **2**, 1437–1444.
48 Y. Ohta, Y. Okamoto, S. Irle and K. Morokuma, *Carbon*, 2009, **47**, 1270–1275.
49 J. C. Charlier, A. DeVita, X. Blase and R. Car, *Science*, 1997, **275**, 646–649.
50 R. Brukh and S. Mitra, *Chem. Phys. Lett.*, 2006, **424**, 126–132.
51 J. P. O'Byrne, Z. Li, S. L. T. Jones, P. G. Fleming, J. A. Larsson, M. A. Morris and J. D. Holmes, *ChemPhysChem*, 2011, **12**, 2995–3001.
52 J. Gavillet, A. Loiseau, C. Journet, F. Willaime, F. Ducastelle and J. C. Charlier, *Phys. Rev. Lett.*, 2001, **87**, 275504.
53 R. Wang, J. Li and Y. Wang, *J. Phys. Chem. C*, 2024, **128**, 5112–5119.
54 P. J. F. Harris, *Carbon*, 2007, **45**, 229–239.
55 Z. Li, L. Deng, I. A. Kinloch and R. J. Young, *Prog. Mater. Sci.*, 2023, **135**, 101089.
56 M. He, S. Zhang, Q. Wu, H. Xue, B. Xin, D. Wang and J. Zhang, *Adv. Mater.*, 2019, **31**, 1800805.
57 Z. Jin, H. Chu, J. Wang, J. Hong, W. Tan and Y. Li, *Nano Lett.*, 2007, **7**, 2073–2079.
58 S. Han, X. L. Liu and C. W. Zhou, *J. Am. Chem. Soc.*, 2005, **127**, 5294–5295.
59 M. S. He, X. J. Duan, X. Wang, J. Zhang, Z. F. Liu and C. Robinson, *J. Phys. Chem. B*, 2004, **108**, 12665–12668.
60 M. Saeidi, *J. Cryst. Growth*, 2014, **404**, 34–38.
61 H. Shahrokhabadi, M. Saeidi, M. Vaezzadeh, H. Shahivandi and M. Salehian, *J. Cryst. Growth*, 2013, **371**, 56–59.
62 H. Yoshida, S. Takeda, T. Uchiyama, H. Kohno and Y. Homma, *Nano Lett.*, 2008, **8**, 2082–2086.
63 H. Ago, N. Ishigami, N. Yoshihara, K. Imamoto, S. Akita, K.-i. Ikeda, M. Tsuji, T. Ikuta and K. Takahashi, *J. Phys. Chem. C*, 2008, **112**, 1735–1738.
64 S. M. Huang, M. Woodson, R. Smalley and J. Liu, *Nano Lett.*, 2004, **4**, 1025–1028.
65 A. Gohier, C. P. Ewels, T. M. Minea and M. A. Djouadi, *Carbon*, 2008, **46**, 1331–1338.
66 Y. J. Tian, Z. Hu, Y. Yang, X. Z. Wang, X. Chen, H. Xu, Q. Wu, W. J. Ji and Y. Chen, *J. Am. Chem. Soc.*, 2004, **126**, 1180–1183.
67 Y. Wang, X. Gao, H.-J. Qian, Y. Ohta, X. Wu, G. Eres, K. Morokuma and S. Irle, *Carbon*, 2014, **72**, 22–37.
68 J. C. Charlier, H. Amara and P. Lambin, *ACS Nano*, 2007, **1**, 202–207.
69 W. Zhou, Z. Han, J. Wang, Y. Zhang, Z. Jin, X. Sun, Y. Zhang, C. Yan and Y. Li, *Nano Lett.*, 2006, **6**, 2987–2990.
70 M. He, T. Yang, D. Shang, B. Xin, A. I. Chernov, E. D. Obraztsova, J. Sainio, N. Wei, H. Cui, H. Jiang and E. Kauppinen, *Chem. Eng. J.*, 2018, **341**, 344–350.
71 M. Saeidi, *Phys. E*, 2015, **70**, 225–230.
72 Y. Hu, L. Kang, Q. Zhao, H. Zhong, S. Zhang, L. Yang, Z. Wang, J. Lin, Q. Li, Z. Zhang, L. Peng, Z. Liu and J. Zhang, *Nat. Commun.*, 2015, **6**, 6099.
73 L. Kang, S. Zhang, Q. Li and J. Zhang, *J. Am. Chem. Soc.*, 2016, **138**, 6727–6730.
74 L. Ding, A. Tselev, J. Wang, D. Yuan, H. Chu, T. P. McNicholas, Y. Li and J. Liu, *Nano Lett.*, 2009, **9**, 800–805.
75 Y. Chen, Y. Hu, Y. Fang, P. Li, C. Feng and J. Zhang, *Carbon*, 2012, **50**, 3295–3297.
76 L. X. Zheng, M. J. O'Connell, S. K. Doorn, X. Z. Liao, Y. H. Zhao, E. A. Akhadov, M. A. Hoffbauer, B. J. Roop, Q. X. Jia, R. C. Dye, D. E. Peterson, S. M. Huang, J. Liu and Y. T. Zhu, *Nat. Mater.*, 2004, **3**, 673–676.
77 S. Zhang, L. Kang, X. Wang, L. Tong, L. Yang, Z. Wang, K. Qi, S. Deng, Q. Li, X. Bai, F. Ding and J. Zhang, *Nature*, 2017, **543**, 234–238.
78 Y. Bai, R. Zhang, X. Ye, Z. Zhu, H. Xie, B. Shen, D. Cai, B. Liu, C. Zhang, Z. Jia, S. Zhang, X. Li and F. Wei, *Nat. Nanotechnol.*, 2018, **13**, 589–595.
79 Z. Zhu, N. Wei, W. Cheng, B. Shen, S. Sun, J. Gao, Q. Wen, R. Zhang, J. Xu, Y. Wang and F. Wei, *Nat. Commun.*, 2019, **10**, 4467.
80 Y. Bai, H. Yue, J. Wang, B. Shen, S. Wang, H. Wang, X. Li, Z. Xu, R. Zhang and F. Wei, *Science*, 2020, **369**, 1104–1106.
81 Z. Zhu, N. Wei, B. Yan, B. Shen, J. Gao, S. Sun, H. Xie, H. Xiong, C. Zhang, R. Zhang, W. Qian, S. Fu, L. Peng and F. Wei, *ACS Nano*, 2021, **15**, 5129–5137.
82 Q. Wen, R. Zhang, W. Qian, Y. Wang, P. Tan, J. Nie and F. Wei, *Chem. Mater.*, 2010, **22**, 1294–1296.
83 B. Peng, Y. Yao and J. Zhang, *J. Phys. Chem. C*, 2010, **114**, 12960–12965.
84 R. Zhang, Y. Zhang, Q. Zhang, H. Xie, W. Qian and F. Wei, *ACS Nano*, 2013, **7**, 6156–6161.
85 P. J. Flory, *J. Am. Chem. Soc.*, 1936, **58**, 1877–1885.
86 X. Wang, Q. Li, J. Xie, Z. Jin, J. Wang, Y. Li, K. Jiang and S. Fan, *Nano Lett.*, 2009, **9**, 3137–3141.
87 T. Inoue, D. Hasegawa, S. Badar, S. Aikawa, S. Chiashi and S. Maruyama, *J. Phys. Chem. C*, 2013, **117**, 11804–11810.
88 J. R. Sanchez-Valencia, T. Dienel, O. Groening, I. Shorubalko, A. Mueller, M. Jansen, K. Amsharov, P. Ruffieux and R. Fasel, *Nature*, 2014, **512**, 61–64.
89 L. Zhu, J. Wang and F. Ding, *ACS Nano*, 2016, **10**, 6410–6415.
90 G. S. Tulevski, A. D. Franklin, D. Frank, J. M. Lobez, Q. Cao, H. Park, A. Afzali, S.-J. Han, J. B. Hannon and W. Haensch, *ACS Nano*, 2014, **8**, 8730–8745.
91 Q. Wang, M.-F. Ng, S.-W. Yang, Y. Yang and Y. Chen, *ACS Nano*, 2010, **4**, 939–946.

92 Y. Xie, L. Qian, D. Lin, Y. Yu, S. Wang and J. Zhang, *Angew. Chem., Int. Ed.*, 2021, **60**, 9330–9333.
93 H. Xie, R. Zhang, Y. Zhang, P. Li, Y. Jin and F. Wei, *Carbon*, 2013, **52**, 535–540.
94 H. Xie, R. Zhang, Y. Zhang, W. Zhang, M. Jian, C. Wang, Q. Wang and F. Wei, *Chem. Commun.*, 2014, **50**, 11158–11161.
95 H. Xie, R. Zhang, Y. Zhang, Z. Yin, M. Jian and F. Wei, *Carbon*, 2016, **98**, 157–161.
96 P.-X. Hou, F. Zhang, L. Zhang, C. Liu and H.-M. Cheng, *Adv. Funct. Mater.*, 2022, **32**, 2108541.
97 A. G. Nasibulin, A. Kaskela, K. Mustonen, A. S. Anisimov, V. Ruiz, S. Kivisto, S. Rackauskas, M. Y. Timmermans, M. Pudas, B. Aitchison, M. Kauppinen, D. P. Brown, O. G. Okhotnikov and E. I. Kauppinen, *ACS Nano*, 2011, **5**, 3214–3221.
98 L. Ding, W. Zhou, H. Chu, Z. Jin, Y. Zhang and Y. Li, *Chem. Mater.*, 2006, **18**, 4109–4114.
99 Y. Chen, D. Ciuparu, S. Lim, Y. H. Yang, G. L. Haller and L. Pfefferle, *J. Catal.*, 2004, **226**, 351–362.
100 D. B. Geohegan, A. A. Puretzky, J. J. Jackson, C. M. Rouleau, G. Eres and K. L. More, *ACS Nano*, 2011, **5**, 8311–8321.
101 X. Liu and L. Dai, *Nat. Rev. Mater.*, 2016, **1**, 16064.
102 T. Y. Ma, S. Dai, M. Jaroniec and S. Z. Qiao, *Angew. Chem., Int. Ed.*, 2014, **53**, 7281–7285.
103 X. Lu, W.-L. Yim, B. H. R. Suryanto and C. Zhao, *J. Am. Chem. Soc.*, 2015, **137**, 2901–2907.
104 R. Cui, Y. Zhang, J. Wang, W. Zhou and Y. Li, *J. Phys. Chem. C*, 2010, **114**, 15547–15552.
105 B. H. Hong, J. Y. Lee, T. Beetz, Y. M. Zhu, P. Kim and K. S. Kim, *J. Am. Chem. Soc.*, 2005, **127**, 15336–15337.
106 X. Qin, F. Peng, F. Yang, X. He, H. Huang, D. Luo, J. Yang, S. Wang, H. Liu, L. Peng and Y. Li, *Nano Lett.*, 2014, **14**, 512–517.
107 Q. Wen, W. Qian, J. Nie, A. Cao, G. Ning, Y. Wang, L. Hu, Q. Zhang, J. Huang and F. Wei, *Adv. Mater.*, 2010, **22**, 1867–1871.
108 M. He, H. Jiang, E. I. Kauppinen and J. Lehtonen, *Nanoscale*, 2012, **4**, 7394–7398.
109 C. Lu and J. Liu, *J. Phys. Chem. B*, 2006, **110**, 20254–20257.
110 Y. Tian, M. Y. Timmermans, M. Partanen, A. G. Nasibulin, H. Jiang, Z. Zhu and E. I. Kauppinen, *Carbon*, 2011, **49**, 4636–4643.
111 Y. Yao, Q. Li, J. Zhang, R. Liu, L. Jiao, Y. T. Zhu and Z. Liu, *Nat. Mater.*, 2007, **6**, 283–286.
112 Y. Tian, M. Y. Timmermans, S. Kivisto, A. G. Nasibulin, Z. Zhu, H. Jiang, O. G. Okhotnikov and E. I. Kauppinen, *Nano Res.*, 2011, **4**, 807–815.
113 A. Bsoul, M. S. M. Ali and K. Takahata, *Electron. Lett.*, 2011, **47**, 807–U894.
114 Q. Jiang, R. Li, F. Wang, X. Shi, F. Chen, Y. Huang, B. Wang, W. Zhang, X. Wu, F. Wei and R. Zhang, *Adv. Mater.*, 2022, **34**, 2107062.
115 A.-L. Wang, X.-J. He, X.-F. Lu, H. Xu, Y.-X. Tong and G.-R. Li, *Angew. Chem., Int. Ed.*, 2015, **54**, 3669–3673.
116 C. Wu, F. Li, Y. Zhang and T. Guo, *Appl. Surf. Sci.*, 2013, **273**, 432–436.
117 X. Shi, S. Zhao, F. Wang, Q. Jiang, C. Zhan, R. Li and R. Zhang, *Nanoscale Adv.*, 2021, **3**, 889–903.
118 R. Li, Q. Jiang, F. Wang, X. Shi, F. Chen, Y. Huang, B. Wang, W. Zhang, X. Wu, F. Wei and R. Zhang, *Small Methods*, 2022, **6**, 2101333.
119 R. Zhang, Z. Ning, Y. Zhang, Q. Zheng, Q. Chen, H. Xie, Q. Zhang, W. Qian and F. Wei, *Nat. Nanotechnol.*, 2013, **8**, 912–916.
120 N. Wei, Y. Liu, H. Xie, F. Wei, S. Wang and L.-M. Peng, *Appl. Phys. Lett.*, 2014, **105**, 073107.
121 L. Cong, Z. Yuan, Z. Bai, X. Wang, W. Zhao, X. Gao, X. Hu, P. Liu, W. Guo, Q. Li, S. Fan and K. Jiang, *Sci. Adv.*, 2021, **7**, eabd2358.
122 Y. Liu, N. Wei, Q. Zeng, J. Han, H. Huang, D. Zhong, F. Wang, L. Ding, J. Xia, H. Xu, Z. Ma, S. Qiu, Q. Li, X. Liang, Z. Zhang, S. Wang and L.-M. Peng, *Adv. Opt. Mater.*, 2016, **4**, 238–245.
123 H. Guo, J. Chen, L. Tian, Q. Leng, Y. Xi and C. Hu, *ACS Appl. Mater. Interfaces*, 2014, **6**, 17184–17189.
124 L. Huang, Y. Liu, G. Li, Y. Song, J. Su, L. Cheng, W. Guo, G. Zhao, H. Shen, Z. Yan, B. Z. Tang and R. Ye, *Nano Lett.*, 2023, **23**, 597–605.